universität wien

MASTERARBEIT / MASTER'S THESIS

Titel der Masterarbeit / Title of the Master's Thesis

„Photocleavable Wings for Proteins: Biomolecular Beam Sources for Quantum Interferometry"

verfasst von / submitted by

Moritz Kriegleder, BSc

angestrebter akademischer Grad / in partial fulfilment of the requirements for the degree of

Master of Science (MSc)

Wien, 2020 / Vienna 2020

Studienkennzahl lt. Studienblatt / degree programme code as it appears on the student record sheet:	A 066 876
Studienrichtung lt. Studienblatt / degree programme as it appears on the student record sheet:	Physik
Betreut von / Supervisor:	Univ.-Prof. Dr. Markus Arndt

Abstract

Quantum interferometry has not only enabled experimental tests of fundamental physics such as the wave nature of matter, it also allows for novel research of complex molecules at the interface of biology and physics. The tools of quantum-assisted metrology aim at revealing optical, electromagnetic, and structural information of biological molecules to high precision. So far, these measurements were limited to small biological complexes such as vitamins and tripeptides. Because of their thermal instability, large biomolecules such as proteins and DNA cannot be volatilised in thermal molecular beam sources.

This thesis describes the development of a novel beam source for soft desorption of electrically neutral proteins. By combining electrospray ionisation and photocleavable molecular tags we created and studied beams of neutral peptides and insulin in the gas phase. I discuss the developmental stages of our photocleavable tags that lead to successful charge state control of biomolecules in the gas phase with ultraviolet laser pulses.

The design can be attached to a wide range of biological macromolecules and could lead to new studies of neutral biomolecules in vacuum. Furthermore, I give an overview of the limitations and possible optimisations of photocleavable tagged proteins.

Abstract

Materiewellen-Interferometrie hat nicht nur unser Verständnis der atomaren Welt präzisiert, sondern uns auch für die Vermessung optischer Eigenschaften von Makromolekülen interessiert. In Experimenten mit Materiewellen können wir Quantenmetrologie von Biomolekülen mit hoher Präzision durchführen und unsere Proben zu den beststudierten Proteinen küren. Bis jetzt waren diese Messungen noch limitiert auf anorganische Moleküle und kleine biologische Komplexe, wie Tripeptide und Vitamine. Wegen ihrer thermischen Instabilität konnten wir größere Biomoleküle bisher nicht volatilisieren - mit unserer herkömmlichen Molekülstrahlmaschine.

Meine Masterarbeit beschreibt die Entwicklung einer neuen Molekülquelle für die sanfte Desorption von elektrisch neutralen Proteinen. Durch die Kombination von Elekrospray Ionisation und photo-spaltbaren Molekülen konnte uns ein Strahl an neutralem Insulin für Experimente dienen. Diese Biomolekülstrahlquelle ermöglicht es uns zum ersten Mal Proteine im Materiewellen Interferometer zu untersuchen. Ich diskutiere also die Entwicklung der photospaltbaren Moleküle mit denen wir die Kontrolle des Ladungszustands mit ultravioletten Laserpulsen versuchen.

Das Design kann an viele biologische Systeme appliziert werden und führt zu neuen Spektroskopiestudien mit neutralen Biomolekülen. Außerdem gebe ich einen Überblick über die Grenzen unserer Methode und mögliche Optimisierungen von photospaltbaren Proteinen aus unseren Kanülen.

Acknowledgements

I would like to express my gratitude to Professor Arndt and the whole Quantum Nanophysics Group for the opportunity to do this project in a cutting-edge research environment. I would especially like to thank Marion, Johannes, Lukas, and Armin for the stimulating discussions and their helpful advice in the laboratory and life. My thanks are also extended to our collaborators of the Mayor group in Basel, especially Jonas with whom I conducted the final experiments on insulin and the quantum administrative office which provided important organisational and personal advice!

I would also like to thank my fellow students and friends that founded with me the Naturwissenschaftscafe to discuss the foundations of science. Flavio, Nino, Emanuel, Thomas, Lucas, and many others helped to organise interesting discussions, events, and a lecture series which had an immense impact on my perspective on physics and the world it is embedded in.

Special thanks to all the music that guided me through these last years. Thanks to Jonas Rodewald, who showed me how to solder guitar equipment, my band mates from Atlantic Collective and Paleblue and to all the artists that provided music to help me study, research and write my thesis: Tame Impala, Blood Orange, Pink Floyd, Miles Davis, Leyya, Radiohead, Falco, David Bowie, HAIM, Tyler the Creator, Bilderbuch, Gorillaz, Prince, Fleetwood Mac, Frank Ocean, Unknown Mortal Orchestra, Funkadelic, Kendrick Lamar, Genesis, King Gizzard and the Lizzard Wizzard, MGMT, Olafur Arnalds, Washed Out, Travis Scott, and Pond.

Finally and most importantly, I wish to thank my parents for their continuous support and repeated encouragement to follow my curiosity. I am especially grateful to Sophie for providing feedback on my thesis, emotional guidance, and that she widened my mindset beyond the borders of my discipline. Without the help of my friends and family, it would have not been possible to finish my master's. Thank you, you know who you are!

Contents

1 Introduction

In 1900, Max Planck described the electromagnetic radiation of a black body by assuming that the energy emitted comes in discrete packets, later termed quanta [1]. His formula was not derivable within classical physics and marked the beginning of the puzzling assumptions that underlie quantum physics. In a similar paradigmatic change Louis de Broglie tackled the old debate if light comes in discrete units or continuous energy. He synthesised the mass energy relation of special relativity and Planck's quantisation relation and postulated that every particle has a wave component [2]. This wave property of matter was first demonstrated in 1927 by Clinton Davisson and Lester Germer [3].

Since then, matter-wave interferometry has proved to be an important tool to study the limits of quantum physics and to do high precision measurements of complex molecules. In 20 years our group extended the range of interferometry from C60 with 721 Da [4] to macromolecules with more than 25 kDa [5].

An additional goal of matter-wave interferometers is to study macromolecules that play an important role in the processes of life such as peptides and proteins with the tools of quantum assisted metrology [6]. Complex molecules such as peptides and proteins are fragile and disintegrate in conventional particle beam sources. To launch them into the gas phase we study novel molecular beam techniques that allow us to manipulate, steer and detect biological molecules in vacuum. With novel interferometry schemes we plan to observe a quantum superposition of insulin which enables the study of optical, structural and electromagnetic properties in vacuum [7].

In this thesis I discuss the design of small molecular tags - the photocleavable tag (PCTs) - that enable us to control the charge state of a protein and has the potential to be used for a novel type of depletion grating in matter-wave interferometry.

In **chapter 2** I present the history and theory of studying biological molecules in the gas phase. Research on molecular beams in vacuum go back to the beginnings of quantum physics and molecular chemistry and has recently been extended into the realm of complex biological molecules.

Our motivation to create beams of peptides and proteins stems from the possibility to do high-precision measurements on vital biological particles in quantum-assisted metrology employing matter-wave interferometry. **Chapter 3** contains the fundamentals of near-field interferometry and the constraints it imposes on our protein beams.

I discuss how to softly volatilise biological molecules into the gas phase in **chapter 4**. While giving an overview of soft desorption methods I discuss how we extended them to control the charge state of molecular beams in vacuum.

In **chapter 5** I present the development of the experimental setup and the results along the way from isolated photocleavable tags over tagged peptides to the successful neutralisation of insulin. Even though we conducted experiments with smaller peptides and insulin, the newest iteration of photocleavable tags is designed to be applicable to a wide range of biomolecules.

In conclusion, I discuss how electrospray ionisation can be modified into a promising beam source of neutral peptides and proteins for matter-wave interferometry in **chapter 6**. In the appendix I summarise thoughts and discussions of the significance of molecule interferometry for quantum foundations. Motivated by the experiments of our group, I had the opportunity to discuss these different perspectives with many researchers from the field that study interpretations of quantum physics to get new insights about the conceptualisation of our studies.

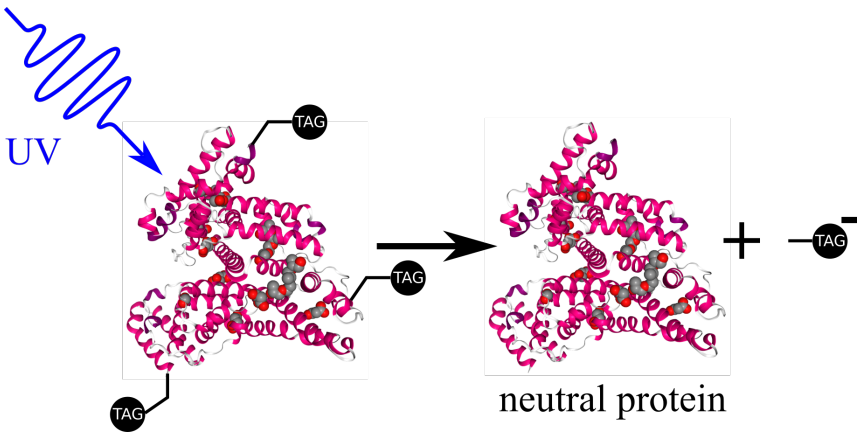

Figure 1: **Protein Neutralisation by UV absorption of photocleavable tags.** *In our experiments, we modified proteins with photocleavable tags to allow for charge state control in the gas phase. The tags attached to proteins absorb a UV photon and fragment at a specific bond. The negative charge leaves the biomolecule with the tag and neutralises the remaining protein.* Provided by Maxime Debiossac.

2 Biomolecules in the Gas Phase

Since the development of molecular biology, the physical foundations of life have been under intense investigation. By assuming that molecules and their interactions explain important mechanisms in biology, physicist Max Delbrück, chemist Linus Pauling and biologists such as Joshua Lederberg and Salvador Luria have motivated many interdisciplinary discoveries [8].

Around the same time, quantum physicists such as Erwin Schrödinger, Niels Bohr and Pascal Jordan speculated about the implications of the new laws of the atomic world for living organisms [9]. Even though many of the speculations that are subsumed under the name of quantum biology are still out of the realm of experimentally testable hypothesis quantum-assisted metrology opened up new possibilities for precise measurements of biological molecules. Additionally, complex molecules of high mass can test fundamental constraints on quantum mechanics such as collapse models [10].

Since quantum-assisted metrology and testing of collapse models relies on gas phase measurements of molecules in a vacuum, we were so far only able to study smaller biological complexes. These can be evaporated in a ceramic oven by heating them up to 460 K thereby generating a molecular beam that can be used in the experiment.

2.1 Molecular Beams

The creation and probing of molecular beams dates back to the theoretical work of Hartmut Kallmann and Fritz Reiche in 1921 [11] and the experimental observations of Erwin Wrede in 1927 [12]. Physical chemists were interested in the deflection of dipolar molecules in inhomogeneous magnetic fields and tested these interactions with beams of diatomic molecules. Motivated by these ideas Stern and Gerlach discovered the spin of silver atoms that was measured as a magnetic moment arising due to a non-classical angular momentum of atoms [13].

Early experiments on atoms and molecules provided ideal tests of quantum phenomena such as space quantisation and spin [14], but they later also turned out to be useful in probing properties of more complex molecules that are essential to the functioning of biological organisms [15]. Molecular Beams can be created by evaporating or heating particles into the gas phase and letting them pass a small opening

slit into a vacuum chamber of low pressure. This acceleration focuses the trajectories of the particles into a straight line which can be manipulated without interactions with background gas. A beam of sufficient intensity and small divergence can then be exposed to electric or magnetic fields that deflect the atoms or molecules according to their electromagnetic properties [16].

For example, we use radio-frequency electric fields to guide peptides and proteins as charged particles through our vacuum chamber. The movement of molecular beams in time-varying electric fields can be described by the phase-space density of the beam in the apparatus. The phase-space density description has the useful property that the number of particles per unit volume stays the same which is given by Liouville's theorem for conservative forces - such as from an electromagnetic potential. Because of this conservation, cooling or decreasing the average velocity of particles in the beam leads also to a reduction in number density. If we start with a high number density of the beam, we have to account for the reduction that follows from cooling that we apply to get the molecules to the desired velocity. A low-velocity particle beam is necessary for high precision spectroscopy and to achieve our goal of quantum-assisted metrology.

To use peptides and proteins in quantum-assisted metrology we have to control the charge state, velocity, angular distribution, and particle intensity of our beam to make it compatible with currently available interferometry setups such as the LUMI experiment that is discussed in **chapter 3**.

2.2 Peptides and Proteins in the Gas Phase

Small and stable particles such as the diatomic molecules of early molecular beam experiments can be transferred into the gas phase by heating but more complex biological molecules such as heavier peptides and proteins fragment under such conditions. This high likelihood of fragmentation of labile compounds has earned these methods the name hard desorption methods. In contrast, the rise of mass spectrometry lead to a renewed interest in soft desorption techniques that leave biological compounds intact. Because of the success in measuring molecular properties in the gas phase and the growing interest in molecular biology we have seen novel methods that allow soft desorption and detection of peptides in vacuum, such as mass spectrometry coupled with Electrospray Ionisation (ESI) and Laser Desorption (LD).

Laser desorption helped mass spectrometry to become a widely used analysis tool from biochemistry to molecule physics and medicine. Posthumus and colleagues showed their potential in early experiments with laser desorption dating back to the late 1970s [17]. In their studies, nanosecond laser pulses on a metal surface volatilised biological compounds such as digitonin with 1228 amu and left them intact in the gas phase. Additionally, they were able to detect nucleotides - building blocks of the most essential biomolecule on earth: DNA.

Nearly two decades after these experiments, Weinkauf and colleagues demonstrated that femtosecond laser pulses are even better suited for desorption and subsequent ionisation of larger molecules [18]. They showed that there are two possible routes to the detection of intact biomolecules in vacuum. Usually, desorption - the transfer of molecules into the gas phase from a solvent or surface - and ionisation - the creation of a charged molecule by electron detachment or attachment - happen in the same step such as in electrospray ionisation. In the experiments of Weinkauf and colleagues, one laser volatilises the molecules and a later laser pulse ionises them in-flight. They argue that shorter excitation times of the ionisation laser leads to smaller variation in the energy distribution and therefore to less fragmentation. Because longer peptide chains consist of the same building blocks in a repeating sequence, many similar fragmentation channels can absorb the photons and break. This is conventionally used in mass spectrometry to identify peptide chains from the signal of the fragmentation pattern. Bigger molecules above 600 amu have more vibrational degrees of freedom and therefore can distribute more photon energy without dissociating. But even if these findings seem promising for our goal of a protein beam source there is also the observation from Schlag and colleagues that ionisation efficiency decreases with increasing molecular weight [19]

In my experiments, I looked at different complexities of peptides - chains of amino acids that are called oligopeptides if they consist of a small number of amino acids and polypeptides if they increase in size. The most interesting polypeptides are proteins that play a vital role in all biological organisms from metabolism to neuronal communication which are ubiquitous in living systems. So ubiquitous that one protein was actually named Ubiquitin because it is present in every eukaryotic cell. We used insulin as protein model for our research because of its small size and well-studied chemical properties.

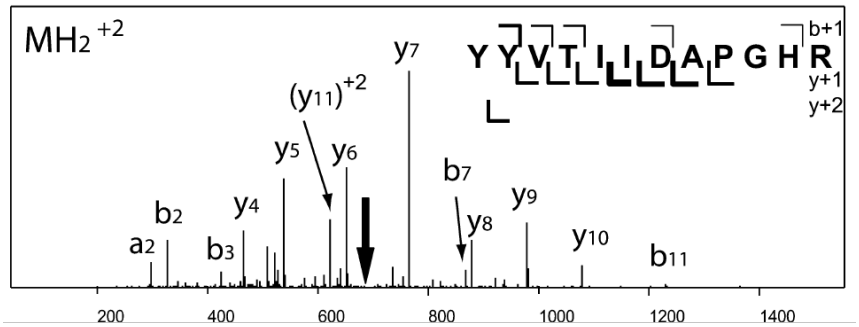

Figure 2: **Identifcation of doubly charged peptides from complex mass spectra.** *The figure shows the complexity of a typical mass spectrum and the main steps to analyse the fragments of the peptide YYVTIIDAPGHR - or Tyrosine - Tyrosine - Valine - Threonine - Isoleucine - Isoleucine - Aspartic Acid - Proline - Glycine - Histidine and Residue. The doubly positively charged ion MH_2^{+2} was selected and dissociated to yield different types of peptide fragments. b labels indicate breaking at the amide bond or the peptide backbone with y being the complementary fragment, a indicates an additional loss of CO with x as counter-part and c and z signals represent extensive cleavage at the peptide backbone. In the right upper corner, the lines show derived dissociation sites where the thickness of the line corresponds to the intensity of the signal. Adapted from [20]*

Previous experiments in our group demonstrated the intact desorption and ionisation of synthesised neutral molecules such as perfluoroalkyl-functionalised tetraphenylporphyrins by laser desorption with nanosecond pulses [15]. These tests were done in a two step process with laser desorption because in contrast to other soft desorption tools, this produces a higher amount of neutral biomolecules that are needed for quantum-assisted metrology.

An additional advantage of gas phase measurements concerns the environmental and solvent effects that chemistry in solution can not exclude. Optical spectroscopy has helped to shine a light on the structure of molecules and their dynamics by observing reactivity and photo-chemistry [21]. For example pulsed-jet expansion has been developed to extend spectroscopy to new size ranges. In such a setup, bigger molecules travel in a pulsed cloud of low-weight molecules that enables the selection of translational velocity and can even provide a cold environment of a few kelvins. We employed a similar technique to volatilise different photocleavable tags (PCTs) that were the first step of development for our novel beam source [22]. Later when studying peptides and proteins we switched to electrospray ionisation for its high efficiency

and continuous molecular beam production.

Because of their high mass-to-charge ratio, electrosprayed peptides and proteins are not suitable for current interferometric setups. Therefore, we had to complement our electrospray setup with a reliable and efficient mechanism to control the charge state of biomolecules. To reduce the number of charges present on bigger peptide chains we used small molecular tags with a photo-active group that absorbs UV photons and uses their energy to break a designated bond between tag and molecule. This technique is called site-specific photodissociation or photocleavage [23].

In biochemistry and medicine, ion activation mass spectrometry enables researchers to look at complex spectra arising when biological tissue is directly analysed. These samples contain a multitude of different molecules in varying concentrations making the identification of signals reminiscent of reading tea leaves. Collisional, optical or thermal activation of the particle beam enables the extraction of informative molecular fingerprints of the sample. For example, peptide chains consist of repeating sequences that enhance the signal of each sequence after reproducible fragmentation which amplifies the signal of the sought-after structure above the forest of background peaks.

Collision-induced dissociation (CID) was the first method that could be applied to a wide range of analytes and is now part of many commercially available mass spectrometers [24]. In CID, particle beams are generated and afterwards transverse a small cell filled with neutral low-weight gas molecules that can be cooled down to a few kelvin in temperature. In time-of-flight mass spectrometry, the beam has a high collision energy of typically a few kiloelectronvolt. But in spectrometers equipped with ion traps, also low collision energies around several electronvolt are feasible. Different collision energies are typically used to activate different ions but we employed this tool in another way to cool the translational temperature of our tested molecules [25].

In contrast to CID, photodissociation works by absorption of either multiple low-energy infrared photons - as observed in infrared multi-photon dissociation (IRMPD) - or with single high-energy ultraviolet photons - methods that are summarised under ultraviolet photodissociation (UVPD). The first photodissociation of molecules has been carried out by Bomse, Woodin, and colleagues in the late 1970s and used an infrared CO2 laser to test the fragmentation behaviour of diethyl ether [26]. These lasers emit light with a wavelength of $10.6\,\mu\mathrm{m}$ which corresponds to a photon energy of $0.1\,\mathrm{eV}$. Because many biological molecules dissociate at an absorbed energy

of several electronvolt, the dissociation only takes place after absorption of 10 to 100 photons [23]. To reduce the charge state of our molecule beam that was softly ionised with electrospray and cooled with collision gas, we used an ultraviolet laser emitting high-energy photons of $4.66\,\mathrm{eV}$. In contrast to CID, photodissociation efficiency has the advantage of being independent of the molecules velocity. This is crucial for our experiment because we aim to cool peptide chains to low velocities to make them viable for interferometry.

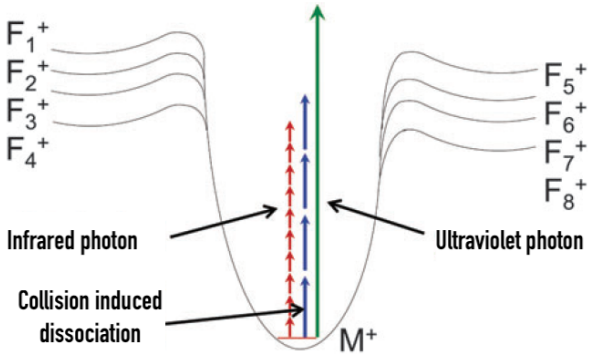

Figure 3: **Comparison of dissociation methods.** *In dissociation spectrometry the energy level of the molecular ion M^+ is raised either by absorbing of multiple infrared photons, a single ultraviolet photon or several collisions. If it crosses the energy barrier sketched left and right, the molecule dissociates into different fragments from F_1^+ to F_8^+. Adapted from [23]*

2.3 Towards Quantum-assisted Metrology

By controlling the charge state, velocity, and phase-space density of biomolecular beams, we aim to widen the class of particles that can be studied in quantum interferometry. In addition to the applications in fundamental physics, we also want to shine light on photochemical properties of peptides and proteins. The recent rise of laser-based experiments on gas phase biomolecules provides a novel link between chemistry and biophysics [27]. This link could be useful in proteomics and medicine to identify and analyse bigger biomolecules and their properties in vacuum [28]. Quantum-assisted metrology could provide high-precision measurements that complement studies with conventional metrology tools [29].

The novel methods of quantum-assisted metrology enable us to determine optical

properties of peptides and proteins to a high-precision by extension of existing technologies. Recent experiments in our group measured the molecular susceptibility, the time-averaged dynamic electric dipole moment, and the molecular optical polarizability of vitamins and showed agreement with computer simulations of the molecular dynamics [6]. Quantum-assisted metrology by deflectometry is achieved by deflecting a molecular beam in a typical quantum interferometer with a high gradient electrode. The visibility contrast that quantifies the typical interference pattern decreases with increasing force acting on the particles and the known deflection force shifts the interference fringes in relation to the static polarisability α_{stat} and electric susceptibility χ. Gring and colleagues also demonstrated how to identify the conformal state of interfered molecules [30].

In order to conduct quantum-assisted metrology in near-field interferometry we have strict limits on our molecular beam source. In the next section, I will outline the fundamentals of near-field interferometry to motivate the requirements for our novel protein beam source.

3 Near-Field Interferometry

We developed our beam source to extend the possibilities of quantum interferometry into the wide range of biological molecules. Hopefully, this will not only extend the exploration of fundamental physics at the interface of life but can also be used to measure molecular properties of vital biological compounds such as proteins and DNA. At the moment, the best candidate interferometry setup is a near-field interferometer with laser gratings such as the LUMI [7]. In this section, I describe the working principle of the setup and which constraints it imposes on the necessary molecular beams.

The original double-slit setup with one grating as envisioned by Young in 1807 [31] is described in the optical far-field - where the distance from the source to the slits is much bigger than the source Aperture A. In the far-field, the curvature of the matter-wave fronts is neglected and the matter-waves are treated as plane waves. This method has been explored with many different classes of particles but its resolution is in principle limited by signal intensity and coherence requirements for the molecular beam [32]. To prepare more massive molecules for quantum interferometry and overcome these limitations, we use a different optical effect that only occurs in the near-field - where the interferometer distances are on the order of the aperture

talbot length $L_A = A^2/\lambda$ and the curvature of the wave front plays an important role. The Talbot-Lau effect is a self-imaging pattern in the near-field with two gratings set at a specific distance, the Talbot length L_T [33]. It consists of the combination of two intriguing optical phenomena that are described below.

3.1 Talbot-Lau Effect

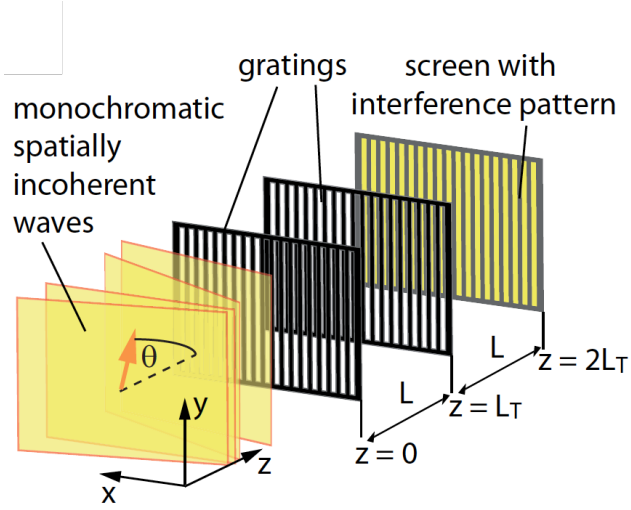

Figure 4: **Talbot-Lau Setup for interference with an incoherent source.** *Monochromatic spatially incoherent waves illuminate two gratings separated by one Talbot length L_T. At the same distance after the second grating, the interference pattern is recovered on the detection screen. The use of incoherent sources for interferometry is possible through a combination of the talbot effect - the self-imaging of the grating structure at L_T - and the Lau effect - the preparation of a coherent beam by an additional grating at the same distance. Adapted from [34]*

The first grating acts as a mask that coherently illuminates the interference grating at the Talbot length. This additional grating is needed because current molecular sources for massive particles are neither bright nor coherent [7]. The constraint on a coherent molecular beam source would reduce the signal intensity significantly due to exclusion of a wide range of velocities. A self-imaging grating helps thereby to create a coherent molecular beam from an incoherent source. This setup is shown in figure 4 the Talbot length can be calculated from the grating period d and the de Broglie wavelength λ_{dB} by the formula

$$L_T = \frac{d^2}{\lambda_{\mathrm{dB}}}. \tag{1}$$

Each slit of the first grating creates a coherent beam that illuminates the second grating if the gratings are set apart by the Talbot length L_T. The second grating creates a characteristic fractal pattern in the optical near field, the Talbot carpet. In figure 5 this pattern was measured with photons in a gas chamber and shows the periodic self-imaging of the grating structure [34]. To be precise, the Talbot effect refers to the self-imaging of the grating in the optical near field and the Lau effect refers to the preparation of a coherent beam by illuminating the first grating with spatially incoherent waves. Our near-field interferometry setup combines both effects, which can be experimentally realised with different types of gratings that are discussed in the next section.

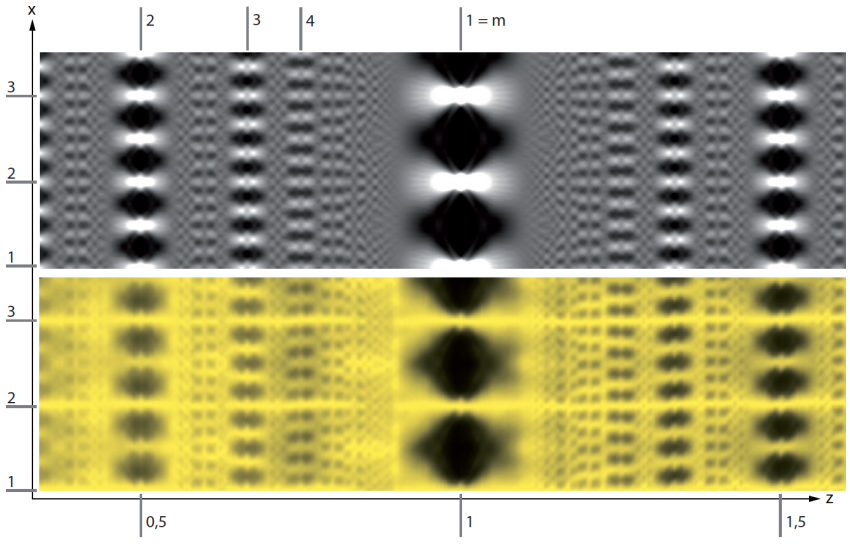

Figure 5: **Talbot carpet measured with incoherent light source.** *The upper panel gives a simulated talbot carpet after illumination of two gratings with an incoherent light source. The calculations predict a periodic self-image after the talbot distance L_T and multiples of it are marked on the z-axis on the bottom of the graph. The lower panel shows the measured talbot carpet in a gas chamber after incoherent illumination of a two grating setup. The top integers m give the order of the self-images. Adapted from [34]*

3.2 Phase Gratings

In interference experiments, material gratings are used to diffract atoms and small molecules which consist of a thin layer of nanofabricated structures in which periodic slits are engraved. The thickness of such a layer can even be reduced to a single atomic sheet of carbon atoms [32].

This interaction blurs the contrast and imposes a limit on the observability of the interference pattern in a matter-wave experiment. Another challenge arises due to the accumulation of particles that start to block the slits and reduce the effective slit width even further. Therefore, we need alternative grating schemes to resolve smaller de Broglie wavelengths for interferometry of peptides and proteins.

To circumvent these limitations we can use the Kapitsa-Dirac effect – the diffraction of matter by a standing light wave. As hypothesised by Piotr Kapitsa and Paul Dirac in 1933, an atom or molecule beam with a de Broglie wavelength $\lambda_{\mathsf{dB}} = \frac{h}{p}$ can be diffracted by a laser [35]. Optical gratings are created by back reflecting a laser beam with a well-defined wavelength λ which creates a standing light wave. This grating-like structure has a periodicity of $\lambda/2$. When the molecular beam transverses the electromagnetic field, the matter-wave acquires a periodic phase shift via the interaction of light and the molecular dipole. The average phase shift is calculated by

$$\Phi = \sqrt{\frac{2}{\pi}} \cdot \frac{P_0\,\alpha}{w_y\,v_z\,\hbar\,c\,\epsilon}, \tag{2}$$

where P_0 is the power of the standing light wave, α the optical polarizability of the molecule, w_y the waist of the laser beam and v_z the molecular velocity in the longitudinal direction [36]. High laser power and a low velocity are therefore necessary to induce a strong phase shift. The phase relation of molecules hitting nodes and anti-nodes of the laser beam leads to an interference pattern at the Talbot length L_T after the phase grating. Thereby, we can indirectly observe the quantum nature of molecules by using an optical grating that does not clog. Additionally, its periodicity can be changed by choosing different laser wavelengths.

3.3 Depletion Gratings

Another possible type of optical grating consists of an ultra-violet laser beam that ionises or fragments molecules in the anti-nodes of the standing light wave [37]. The electrically charged or fragmented molecules can then be removed from the beam by applying an electric field or mass selecting only intact particles. This creates a periodic pattern in the beam which shows interference fringes in the detector comparable to phase gratings. So far, this scheme has been used to study interferometry of whole molecule clusters in the time-domain and is promising to work for metal clusters of up to 300 kDa [7].

For future interferometry setups, this mechanism could act as the first grating which provides coherent illumination of the diffraction grating by the Lau effect described befor. A standing light-wave like this circumvents the common problem of clogging material slits. The only limitation of this type of grating is the different ionisation energies needed for depletion or fragmentation of different molecules and clusters. Although this can be solved by modifying particles with a functional group that allows to ionise or fragment all tagged compounds. In this thesis, I discuss a slight variation of the concept with tagged polypeptides and insulin that depletes the beam by photo-cleavage – the fragmentation of a specific bond by an UV-photon.

3.4 Detection Schemes

Through the development of a new type of interferometry that enables interference measurements on biological molecules, another bottleneck became clear: the detection. In earlier experiments, the detection of molecules was achieved by ionisation and counting in a quadrupole mass spectrometer (QMS). This scheme was implemented by adding a third grating after the diffraction grating that could be moved to scan the interference fringes. Because the mass spectrometer has no spatial resolution, the beam intensity was further reduced by adding this third grating. Due to the low ionisation efficiency, the measurement of interference takes several times longer to record significant visibility contrast. So far, the detection of neutral proteins in the gas phase is still an open challenge.

Another proposed detection scheme with higher efficiency is the collection of the molecules on a glass slide and subsequent imaging by fluorescence detection. In this scheme, biological specimens are excited by a laser beam and emit fluorescence

photons which can be detected with a CCD camera. Novel extensions of this method even allow for resolution below the optical Abbé limit [38]. If the interference pattern is recorded in the distribution of particles on the surface, the slide only needs to be scanned by a tightly focused laser beam that stimulates fluorescence to recover a 2-dimensional image from which the visibility can be calculated. By tagging the particles with a molecular structure that always fluoresces at a specific wavelength, we would have a more efficient and universally applicable detection scheme for neutral biomolecules.

A recent interest in interferometric imaging lead to the development of a new detection scheme called interferometric scattering microscopy (iSCAT). iSCAT imaging works by interfering the light scattered from a sub-wavelength object with a reference light field. The light intensity I_d that hits the detector can be described by

$$I_d \propto| \overline{E_r} + \overline{E_s} |^2 = I_r + I_s + 2E_r E_s cos\phi \tag{3}$$

with $\phi = \phi_r - \phi_s$. The scattered electric field from the object is given by $\overline{E_s} = E_s e^{i\phi_s}$ and the reference field by $\overline{E_r} = E_r e^{i\phi_r}$ [39]. This equation describes many different imaging schemes by proper definition of $\overline{E_r}$. For example in the common bright-field microscopy the reference electric field $\overline{E_i}$ consists of $\overline{E_i} = E_i e^{i\phi_i}$ the background light that hits the object to be imaged. An extension for iSCAT imaging employs the use of a partially reflective plate to interfere the scattered light with a back-reflection of the beam. In this case, the reflective index scales the illumination field by $\overline{E_r} = r\overline{E_i}$. iScat schemes described with the above equation have already been used to image vital biological functions in a non-invasive way, such as native proteins secreted from living cells, viruses and DNA [40].

In our photocleavage experiments, we used a Time-of-Flight Mass Spectrometer (TOF-MS) to detect ionised particles. In a TOF-MS, ions are accelerated by a fixed potential U and then travel a distance d in free-flight [41]. For a molecule with the charge state q, the mass can be calculated from

$$m = 2q\,U \left(\frac{d}{t}\right)^2 . \tag{4}$$

Because of the fixed potential U and flight length d, ions of different mass need dif-

ferent times t to travel to the detector. By separating the molecular beam in pulses, a wide range of different particles can be analysed at the same time to record a mass spectrum that gives mass-to-charge ratios m/z of the molecules. This TOF-MS could be coupled to near-field interferometers to record the interference pattern of biomolecules. But since interferometry of bigger molecules in our setups works with neutral particles it would make post-ionisation of the interfered particle beams necessary and ionisation efficiency scales inversely to particle mass [19].

3.5 Protein Interference

The goal of my thesis is to develop and describe a novel source method for neutral protein beams in high vacuum. This would enable quantum interferometry of proteins if the molecular beam fulfils certain characteristics to be compatible with current near-field interference setups. First, the particles need to be electrically neutral to reduce interactions with the diffraction gratings and avoid decoherence by forces from electrical or magnetic fields in the vacuum chamber. Second, the beam has to be sufficiently cold to reduce decoherence through the emission of thermal photons. Third, the particles need to have the right velocity to create interference fringes in a spatial interferometer. High velocities result in small de Broglie wavelengths and very slow molecules get accelerated downwards by gravity and will not reach the detector.

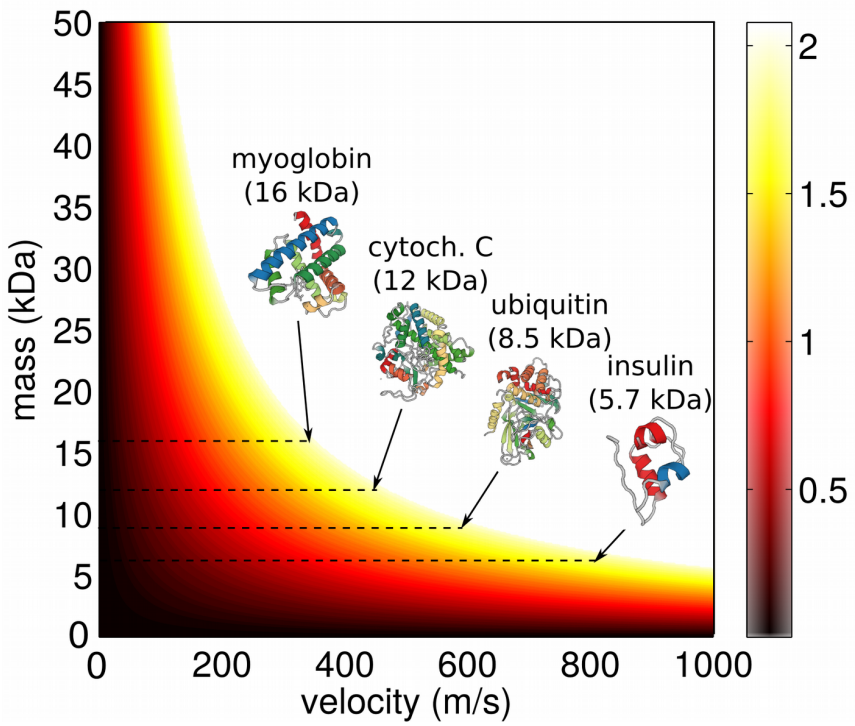

Figure 6: **Comparison of velocities needed to observe protein interference in near-field interferometry.** *The colour bar represents the interferometer length, where the white region $L > 2\,\mathrm{m}$ shows values that are not achievable with current interferometers. This figure was provided by Maxime Debiossac.*

Figure 6 gives an overview of the tight constraints on a molecular beam source for proteins with increasing mass. Small proteins such as insulin would need to be decelerated to $800\,\frac{\mathrm{m}}{\mathrm{s}}$ or less to show interference in matter wave interferometers below two meters of length. With proper collision gas pressure a low velocity spread of down to 1 eV for myoglobin is possible [42]. The internal temperature of molecules can be cooled down by collisions of buffer gas at cryogenic temperatures of $4\,\mathrm{K}$ [43]. This would thermalise proteins in our buffer gas cell of 10 cm length to temperatures well below $70\,\mathrm{K}$. The goal is to create a protein beam with over $100\,\mathrm{counts/s}$ with a divergence angle below $1\,\mathrm{mrad}$.

Our strategy involves starting with a beam of biomolecular ions which can be controlled in velocity and collimation. Subsequently, we have to neutralise the ions to perform interferometry. I discuss the methods we employed to generate neutral beams in **chapter 4** and the results of our experiments in **chapter 5**.

Besides metrology, there are other reasons to further push the limits of interferometry with complex molecules. Through understanding the interactions of a mesoscopic quantum state with the experimental setup, we can study how different measurements and environmental effects influence the transition from quantum to classical states. We can experimentally test the border at which the indeterministic and non-local laws of quantum physics turn into the deterministic and causal world of classical mechanics [10].

4 Molecular Beam Sources

Quantum experiments with biological molecules so far have been limited to small complexes such as tetraphenylporphirin [44] and vitamins [6]. Matter-wave experiments have already demonstrated interference of even bigger artificial molecules [45], but proteins have so far not been used in these setups. The problem lies in creating a sufficiently cold and intense beam of biological molecules that can be used to observe interference contrast. In this chapter, I describe a beam source method that we tested with several peptide chains of different lengths and insulin, a well-studied protein that is commercially available not only to diabetics.

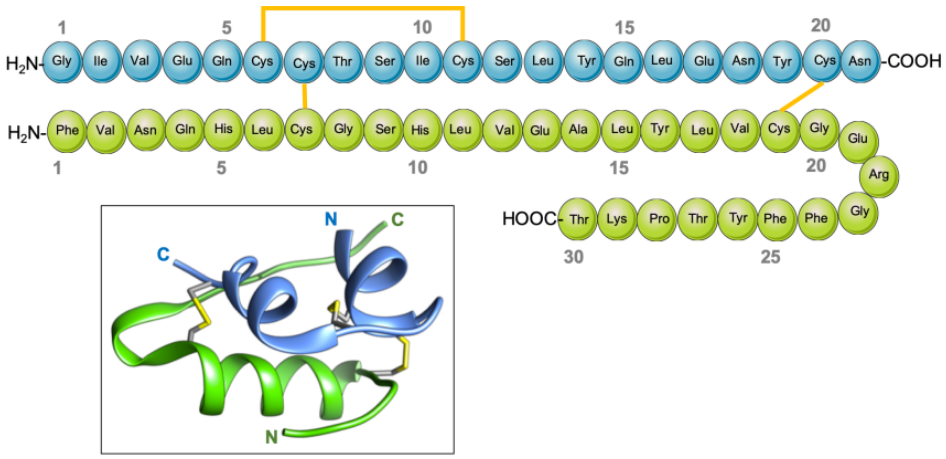

Figure 7: **Structure of Insulin.** *The protein insulin consists of two chains connected by disulphide bridges at the amino acid cysteine. The upper A-chain is drawn in blue and the lower B-chain in green. The inset shows the typical 3D folding structure and the yellow bridges connect the two chains.* Reprinted from [46]

Insulin is a small polypeptide with a molecular mass of 5733 Da in its bovine form, which is a good model candidate for a new protein beam source. It consists of 51 amino acids and has been detected through ionisation methods already 30 years ago [47]. Because of its low mass and high thermal stability in contrast to larger protein complexes, we chose it as proof of principle for our novel protein beam source. The range of hypothetical protein candidates goes up to the biggest known natural protein in the human body: Titin with over 34000 amino acids and a mass of more than 3.8 MDa [48].

In our experiments, we manipulate the molecular beam with a UV laser of 266 nm

to change the charge states and later plan to use it as a standing light-wave grating. Therefore, it is important to understand the interaction between UV laser light and the amino acids that make up proteins. Tryptophan, Tyrosin and Cystine are known to absorb photons of wavelengths in the vicinity of our used laser beam at 266 nm [49]. The molar absorption coefficient ϵ is a useful parameter to calculate the absorption cross-section σ of a protein. From solution experiments, we know that it can be estimated by

$$\epsilon_{280}(M^{-1}cm^{-1}) = \#Tryptophan \cdot 5500 + \#Tyrosine \cdot 1490 + \#Cystine \cdot 125, \quad (5)$$

where # denotes the number of the specific amino acids occurring in the polypeptide. From ϵ_{280} we can predict the absorption cross-section σ by the relation

$$\sigma = \frac{\epsilon \; log10}{N_A}. \quad (6)$$

We use this parameter to predict the interaction between UV laser light at 266 nm and the peptides and proteins. The wavelength from literature is close enough to calculate a rough estimate that we can compare to our measured data. The exact absorption cross-section σ depends on factors that we can not control in our experiment. The most prevalent source of uncertainty is that the amino acid histidine also absorbs at this wavelength, but only in a certain conformation. Because we can not test or control the conformation of histidine, we neglect its influence to derive an approximation for the absorption cross-section of native insulin $\sigma_{\text{Ins}} = 2.57 \cdot 10^{-20}\,\text{cm}^{-2}$ for native insulin. In comparison, our neutralisation mechanism relies on a small molecular tag with strong absorption in the ultraviolet. This photocleavable tag has an absorption cross-section $\sigma_{\text{pc}} = 4 \cdot 10^{-17}\,\text{cm}^{-2}$, which is three orders of magnitude higher and therefore absorbs most of the photons when tagged proteins are exposed to UV radiation. Additionally, several tags on each biomolecule further increase the photocleavage efficiency.

In interferometry, neutral molecules are used to reduce interactions of particles with the gratings and with each other to avoid decoherence. If the studied particle beam is created by thermal evaporation, enough neutral molecules are desorbed

to perform interferometry experiments. But this source mechanism has limitations. Heating of biomolecules leads to fragmentation of complex structures such as proteins. This creates a wide distribution of substructures which reduces the signal of the intact parent molecule.

Therefore, we investigated two well-known methods from mass spectrometry that softly desorb particles into the gas-phase: Electrospray Ionisation and Matrix-assisted laser desorption. Both tools create charged molecules that can be controlled, cooled and detected in the gas-phase. This enables us to steer the ions and change the beam parameters in vacuum. But to perform interferometry we need to neutralise the ion beam, which we achieve by photocleavable tags as discussed in **chapter 5**.

4.1 Electrospray Ionisation

Mass spectrometry is a widely used detection method to determine the mass-to-charge ratio of molecular compounds. But before the late 1980s, it was limited to low mass molecules because of the lack of soft desorption techniques available that allowed for intact desorption and detection of biomolecules. Electrospray ionisation (ESI) enabled the production of molecular beams and detection of intact macromolecules in the gas-phase. In 1968, Malcolm Dole and colleagues demonstrated a functional ESI [50], but it took 20 years of refinement until John Fenn and colleagues could detect intact biomolecular ions in the gas-phase [47]. This novel tool was efficient in creating high-intensity beams of biological compounds and became a standard technique for nearly every mass spectrometry department in the world and John Fenn was awarded the Nobel prize for it in 2002 [51].

In our experiment, we use a commercial Waters electrospray ionisation mass spectrometer (ESI-MS) to generate and detect a beam of biomolecular ions. ESI starts with a solution of dissolved particles in a syringe, which are sprayed through a capillary with a diameter of $500\,\mu$m. A voltage of 2-$3\,$kV is applied to the capillary and the liquid is accelerated to a counter electrode at the entrance of the vacuum chamber. The coulomb repulsion of the charges in the droplet is competing with the surface tension that acts to keep the liquid in the capillary. At the right voltage, these forces are in equilibrium and the fluid is sprayed in the form of a pointed cone. This effect is named after Sir Geoffrey Taylor who showed that the equilibrium state can only be maintained in a cone shape with an opening angle close to $49,3^\circ$ [52].

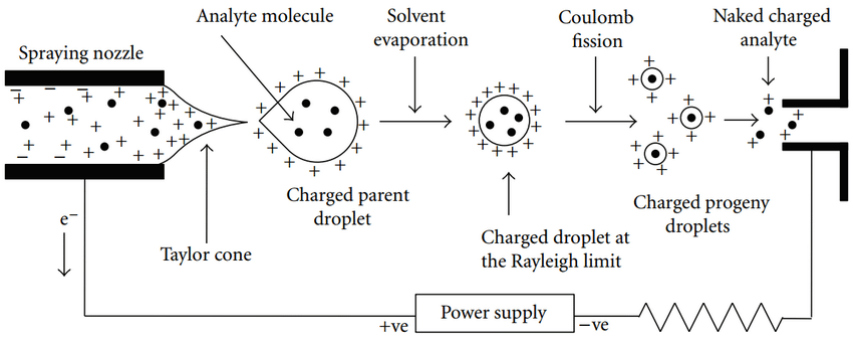

Figure 8: **Sketch of the Electrospray Ionisation mechanism.** *First, free charges form in the capillary. Second, a Taylor cone forms and creates charged primary droplets. Then sheath gas and a high temperature lead to solvent evaporation. Smaller secondary droplets are generated through Coulomb fission and at the final stage, individual ions enter the vacuum chamber. Adapted from [53].*

Figure 8 shows a sketch of the ESI mechanism. At the start, electrochemical reactions such as oxidation and solvent create free charges inside the steel capillary. The high voltage leads to the formation of a Taylor cone which produces charged primary droplets. A stable jet can only be maintained at a specific voltage that balances out the surface tension.

In a systematic study, four modes of spraying have been observed [54]. At low voltages and solvent flow rates, the liquid drips out irregularly. With increasing Coulomb attraction a stable cone jet forms. If we apply an even higher voltage, the stable jet splits into several droplet jets that still produce a detectable signal of ions. After further increase of voltage and flow rate, the spray becomes unstable and is referred to as entering ramified-jet mode.

The droplets in the Taylor cone only consist of a limited number of charged particles, because with the increase of charges the coulomb repulsion becomes strong enough to disperse the droplets. The maximum number of charges q in a stable droplet is called the Rayleigh limit and can be calculated by

$$q = 8\pi \sqrt{\epsilon_0 \, \gamma \, r^3}, \tag{7}$$

where ϵ_0 is the vacuum permittivity, γ is the surface tension, and r denotes the droplet

radius. Because of surface tension ESI does not create a stable spray with water. Therefore, other solvents such as ethanol and acetonitrile have to be used.

To evaporate solvents in the droplets, we used a sheath gas flow from 20-400 $\mathrm{L/hr}$ around the capillary and the source was at a temperature of 100 $^\circ\mathrm{C}$ to further assist the evaporation. Because the solvent molecules leave the droplet neutrally, the number of charges stays the same, but the radius decreases. This leads to a higher electric field density, which in turn disperses the droplets in a coulomb explosion into multiple nanodroplets that have a diameter on the order of 200 nm [55]. In comparison, the primary droplet size is on the order of 1 μm.

Even though ESI is a common molecular analysis tool, the exact mechanism of ion formation is still debated [56]. The two most common explanations are the charge residue model and the ion evaporation process. Right after the invention of ESI-MS, Dole and colleagues proposed that every charged, secondary droplet contains only a single target molecule [50]. This observation was important to construct the full charge residue process. In their model, a micrometer-sized droplet forms directly after spraying and the sheath gas leads to further evaporation of the solvent. If the Rayleigh limit is reached, the droplet forms a Taylor cone and emits nanodroplets that contain a single ion. After full evaporation of the solvent, the individual ion remains in the mass spectrometer. To understand this mechanism, it is important to note that a Taylor cone forms both at the end of the capillary and in each evaporating droplet.

The other proposed mechanism is called the ion evaporation model. Originally developed by Iribarne and Thomson, it explains the ion formation by individual ions leaving the charged droplets in flight [57]. According to their explanation, secondary droplets emit ions to compensate for the increasing electric field strength on the surface. This happens continuously at a reaction rate k_{react} until the droplet is fully evaporated [55]. With the Boltzmann constant k, temperature T, Planck's constant h, Gibbs energy G and the ideal gas constant R we can calculate the rate of emission

$$k_{react} = \frac{kT}{h} \cdot e^{-\frac{\Delta G}{RT}}. \tag{8}$$

The ion evaporation model proposes that ions are desorbed from a solvent droplet. In contrast, the charge residue model assumes that droplets of solvent and a single ion evaporate until the individual ion remains [58]. The main difference between the two models is therefore how individual ions are formed after several stages of evaporation

and droplet separation.

According to Wilm and colleagues, the current consensus in physical chemistry is that small ions are generated by ion evaporation and large ions above 1000 Da by the charge residue process [55].

Another proposed mechanism compares folded and unfolded proteins of different sizes. The so-called chain ejection model assumes that unfolded proteins and other big polymers show different behaviour in ESI as the two processes described above. By molecular dynamics simulations, Konermann and colleagues found that compact polymers tend to act hydrophilic and extended chains show hydrophobic behaviour [56]. The unfolding therefore leads to migration to the surface and subsequent ejection of the ion from the solvent.

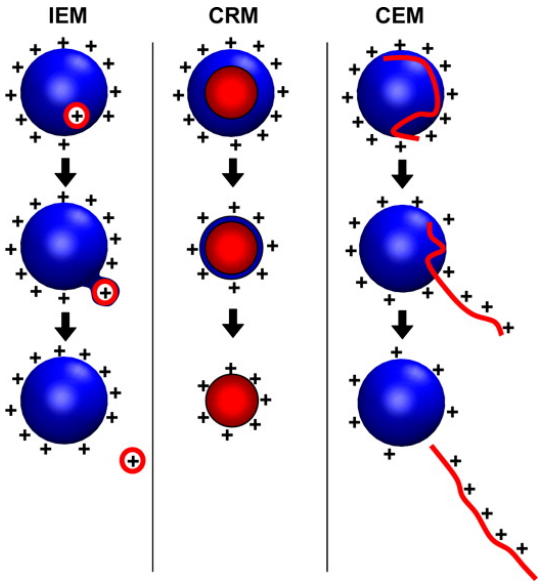

Figure 9: **Comparison of possible electrospray ionisation mechanisms.** *On the left, the Ion Evaporation Model (IEM) assumes that individual ions leave the charged primary droplet in-flight. In the middle, the Charge Residue Model (CRM) states that secondary droplets with only a single ion inside are created and after solvent evaporation, the ion is isolated in the gas-phase. On the right, the Chain Ejection Model (CEM) explains that bigger biopolymers such as unfolded proteins leave the charged droplet because of their hydrophobic properties. Adapted from [56]*

In our experiments, we studied the behaviour of peptide chains up to small proteins such as insulin. According to the literature presented, the ions of smaller peptides are

created by the ion evaporation mechanism and larger compact protein ions arise due to the charge residue process. For increasingly massive proteins we expect to create biomolecular ions that unfold according to the chain ejection model. Even though the exact process of ESI is still discussed, which mechanism actually takes place is not crucial for our experiments. So far, we were able to ionise and detect all possible biomolecular candidates for interferometry.

A novel refinement of the general method is nano-electrospray, which primarily produces nanodroplets of comparable size without relying on secondary droplet formation as in conventional ESI described above. In this source mechanism, a small capillary of $1\,\mu\mathrm{m}$ and a low spraying speed of around $20\,\mathrm{nl/hr}$ is used to increase ionisation efficiency up to 100% [59]. Even though, the high efficiency and low solution consumption is a big advantage of nano-electrospray, we used the classic ESI approach for our experiments. After preliminary studies, we observed that nano-electrospray needs more maintenance because the capillaries clog more easily and sample consumption was not an issue for our study.

4.2 Matrix-assisted Laser Desorption Ionisation

A second soft desorption technique that we tried is Matrix-assisted laser desorption ionisation (MALDI). In comparison to ESI it produces mainly singly-charged molecules but also volatilise proteins with higher velocity. Karas and colleagues discovered in the 1980s that non-absorbing amino acids such as alanine could be ionised by adding tryptophan that absorbs laser light at $266\,\mathrm{nm}$. This so-called matrix molecule is mixed with the target molecule in solution and applied to a solid surface. The solvent evaporates and the matrix and target form a thin layer of particles. By irradiation with a pulsed UV laser, the matrix absorbs energy and ablates the target molecules. By addition or subtraction of protons, the initially neutral molecules are ionised and can be detected in a mass spectrometer [60]. In contrast to ESI, MALDI produces mostly singly charged molecules.

Even though MALDI is widely used in scientific and commercial applications the mechanism behind it is not fully understood [61]. One of the proposed models explains it by looking at the combined physical and chemical interactions of the matrix and target molecules. According to the Coupled Chemical and Physical Dynamics (CCPD) model, the ionisation takes place in three steps: First, matrix molecules are

in the electronic ground state S_0 and get into the excited state S_1 by the absorption of a UV photon:

$$S_0 + h\nu \longrightarrow S_1 \tag{9}$$

Second, the photoexcited molecules pool together in the matrix and form higher excited states S_n through collision:

$$S_1 + S_1 \longrightarrow S_n + S_0 \tag{10}$$

Third, the higher excited states S_n collide with other excited molecules and set electrons free:

$$S_n + S_1 \longrightarrow M^+ + e^- + S_0 \tag{11}$$

Free electrons are captured by matrix molecules and create additional anions. After formation, the anions and cations form protonated/deprotonated ion pairs which are highly reactive and ionises the target molecules.

MALDI produces a mixture of several compounds such as molecular anions, cations, and clusters of molecules. By proper mass selection it is possible to select single species and create a lowly-charged molecular beam. This enabled the analysis of big proteins in the gas-phase up to $100\,\mathrm{kDa}$ and Tanaka shared the 2002 Nobel prize with Fenn [62]. Interestingly, both of these methods work by addition or loss of a proton from the molecule, also called protonation and deprotonation. Before, ionisation was defined as acquiring a charge through losing an electron or capturing a free electron from the environment.

In our experiments, we wanted to employ MALDI for modified Proteins such as tryptohphan-tagged ubiquitin but did not follow up on this method because of the low intensity of the recorded signal. But since other laboratories already reported successful detection of ubiquitin and complex modifications, this method could be important in future extension of our setup [63].

4.3 Charge Reduction of Peptides and Proteins

In the previous section, I discussed different methods to volatilise and detect fragile biological molecules such as peptides and proteins. Before the development and refinement of soft ionisation methods, it was impossible to study biomolecules without the interaction of a solvent or intermolecular reactions. Even though these new methods enabled the study of gas-phase ions, we still can not use them for quantum interferometry because of their electric charge. In our experiments, we combined the advantages of soft ionisation with a new mechanism that allows us to reduce the charge state of peptides and proteins to create a cold, collimated and electrically neutral beam of macromolecules.

The novel design, which was developed together with the Mayor group, consists of a small molecular tag that is attached to the target particle and interacts with a UV laser pulse in a well-controlled manner. By splitting off a specific part of the tag with an electric charge, we can reduce or increase the charge state of a host molecule. Such photochemical methods are highly useful for us, because we operate in high vacuum conditions where only a small amount of background molecules are present and intermolecular interactions are rare. To give an overview of the different possibilities of photochemistry, I explain different types of light-molecule interaction. All of them can be subsumed under the term photodepletion, the reduction of beam intensity through interaction with photons.

Mass spectrometry is a useful tool to analyse the components of a sample but is limited by the complexity of the recorded spectra. Large biomolecules often exhibit diverse signal of multiple charge states in spectrometry which makes it difficult to assign specific fragments and identify compounds. Photodissociation, or the fragmentation of molecules by interaction with light, turned out to be a helpful tool to tackle this problem. By coupling a laser into a mass spectrometer, it is possible to influence the mass spectrum in real-time and fragment big biomolecules into analysable smaller compounds.

Deterministic fragmentation channels revealed structural and sequential information and researchers use different laser wavelengths to study optical properties of molecules such as absorption cross-section [23]. As discussed in **Chapter 2**, the new technique of photodissociation mass spectrometry became central in biochemistry fields such as proteomics and drug discovery. The two most common applications are Infrared Multiphoton Photodissociation (IRMPD) and Ultraviolet Photodissociation

(UVPD).

In comparison to IRMPD, UVPD excites the target molecules much faster and creates a richer fragmentation pattern [64]. The high energy UV photons deposit much more energy and dissociate the analyte right after excitation. The timescale of such a fast reaction is on the order of femtoseconds [64]. Additionally, amino acids with aromatic side-chains such as tryptophan, tyrosine, and phenylalanine have a high dissociation efficiency. This allows for UVPD of many peptides and proteins such as insulin and is used to identify unknown proteins in proteomics [23].

Another method that fragments molecules for the analysis of mass spectra is Collisional Induced Dissociation (CID) [65]. In contrast to photodissociation, CID is much easier to implement because it only consists of a chamber filled with buffer gas. The molecular beam collides with the buffer gas and dissociates through multiple collisions. Usually, the buffer gas can be controlled in temperature – such as in our experimental setup – which enables cooling of the target compounds.

Our group also studied a new kind of quantum interferometry grating type, which builds upon the mechanism of UVPD: photofragmentation gratings [37]. In the OTIMA (optical time-domain matter-wave) experiment, 157 nm vacuum ultraviolet (VUV) lasers are used to fragment molecular clusters and biomolecules to extract charged fragments from the beam. The very high photon energy of 7.9 eV is necessary so that a single photon is sufficient to ionise or fragment the target compounds, which pass the optical VUV grating only for a short period of time. In contrast, photoionisation gratings do not work with large biomolecules because the particles exhibit high ionisation energies which cannot be reached with UV table-top lasers [37]. Such high single photon energies can only be achieved with synchrotron radiation. In contrast, photofragmentation gratings are not limited to small particles with low ionisation energies.

In general, photodissocation can be used for protein interferometry but is not a deterministic way of neutralisation. The position of the charge on biomolecules can be delocalised and the dissociating bond is different for the studied species. To develop a reproducible neutralisation mechanism we have to localise the charge to a certain degree and remove it from the protein with high efficiency.

Before I present the main focus of our research – the photocleavable tags – I will discuss the steps necessary to conduct photoneutralisation by photocleavage. A singly tagged molecule can only emit a single charge by absorption of UV photons.

Therefore, we had to implement a method that reduces the charge state of ESI protein beams to one.

After preliminary tests, we developed a corona discharge source that enabled us to study singly charged insulin beams of sufficient intensity. This source is described in the following section before I discuss alternative approaches and their limitations.

4.4 Corona Discharge

Charge Reduction Electrospray Mass Spectrometry (CREMS) was first developed to increase peak separation and thereby decrease spectrum complexity of the observed mass spectra. The goal was to reduce charge states of big proteins such as haemoglobin with a mass of $64\,\mathrm{kDa}$. In conventional ESI, such big complexes gather approximately 16 charges during soft desorption and due to fragmentation, clustering, and background noise the observed peaks become difficult to assign to the right compounds [66].

In our case, we experimented with smaller proteins from insulin at $5.7\,\mathrm{kDa}$ to myoglobin at $17\,\mathrm{kDa}$. But already these analytes acquire multiple charges in the ionisation process. Intriguingly, ESI-MS detects most of the proteins in the range from $500 - 2000\,\mathrm{m/z}$ [67]. As a simplified rule, we see that proteins acquire roughly one charge per $1500\,\mathrm{Da}$. Of course, this is an oversimplification and the actual behaviour depends on the specific compound and spraying conditions.

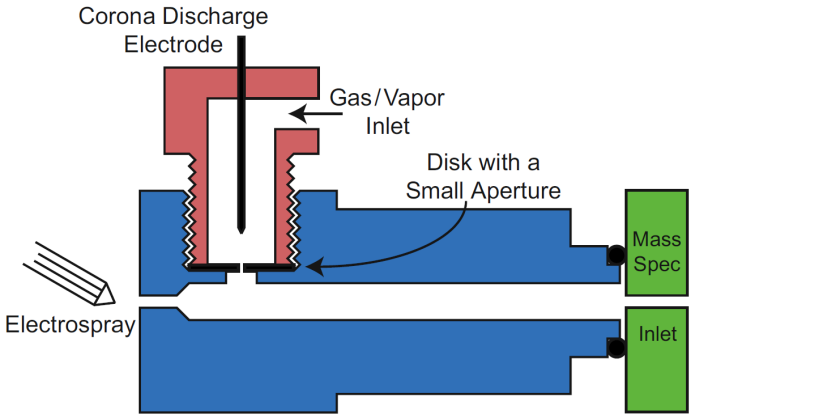

Figure 10: **Sketch of a corona discharge chamber.** *A platinum wire at the top electrode is set to a high voltage and ionises the gas molecules which enter the ionisation chamber (red). A small aperture lets ions of the right polarity into the interaction chamber (blue). The electrosprayed biomolecule ions enter the interaction chamber from the left and collide with ionised gas. This reduces their charge state to create singly charged proteins that enter the mass spectrometer on the right. Adapted from [68]*

To enable photoneutralisation of proteins we studied different approaches of charge reduction to a singly charged state. From this stage, we would be able to test the potential of the PCT to create a neutral biomolecular beam.

The most promising method was charge reduction in a corona discharge chamber that is described in this section. In positive ESI mode, proteins acquire charges through protonation. Therefore, the direct way of charge reduction would consist of a proton transfer reaction that again removes the donated protons in free-flight. In our experiment, this is achieved through gas-phase anions that collide with the protein cation beam and capture protons. By changing the polarity of the voltages and the ESI mode it is also possible to charge reduce protein anions by gas cations.

Corona discharge creates gas-phase ions by a strong electric field in a small chamber filled with gas. In our case, a platinum wire is connected to a high voltage source set to a potential of 2 kV and a steel plate on the other side acts as counter electrode [69]. The high voltage of the wire ionises the gas in the chamber and the ions exit the chamber through a small pinhole in the steel plate. Behind the pinhole, the protein beam flows from the syringe into the mass spectrometer. We call this

interaction region the neutralisation chamber and the setup is sketched in **figure 10**.

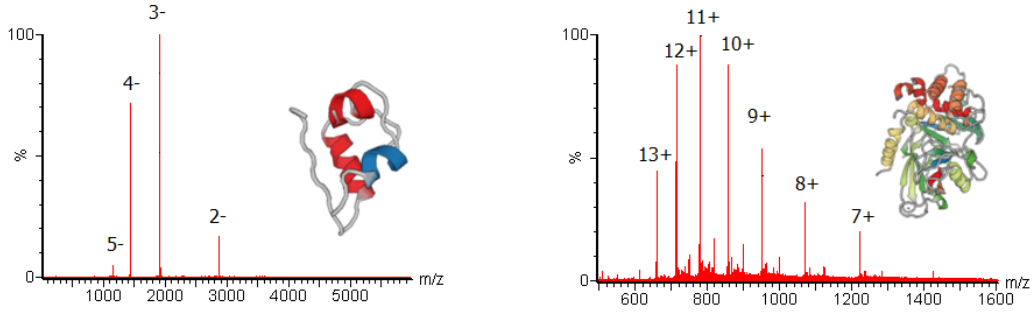

Figure 11: **Charge states of proteins in electrospray ionisation.** *On the left, we show the multiple charges insulin molecules with a mass of* $5.7\,\mathrm{kDa}$ *acquire in our electrospray mass spectrometer. On the right, the bigger protein ubiquitin with a mass of* $8.5\,\mathrm{kDa}$ *is shown. Because of the high abundance of multiply charged biomolecules, we employed corona discharge to charge reduce our analytes.*

In the corona discharge chamber, a high voltage source produces a plasma by ionising gas in the chamber. The plasma consists of positive ions and free electrons for both positive and negative polarity but the charge reduction mechanisms are different. A positive wire attracts free electrons which collide with neutral gas molecules. This creates mostly O_2^+ and N_2^+, which get repelled from the positive wire and enter the neutralisation chamber [70]. A wire on a negative voltage, in contrast, accelerates electrons in the opposite direction. Neutral molecules capture these electrons and enter the neutralisation chamber as O_2^- and N_2^- [68].

We designed and built the corona discharge chamber from the ground up based on previous work which found the interaction time of ions to be around $5\,\mathrm{ms}$ [69] nice. For the most efficient charge reduction, we applied a voltage of $2500 - 3100\,\mathrm{V}$ to the platinum wire and used between $10 - 80\,\mu\mathrm{A}$. The exact values vary due to different spraying conditions and alignment of the wire. The charge reduction efficiency also depends on the gas flow through the ionisation chamber. Higher flow rates lead to a lower average charge state in the molecular beam. Figure 12 shows the effective charge reduction of the proteins GFP and myoglobin

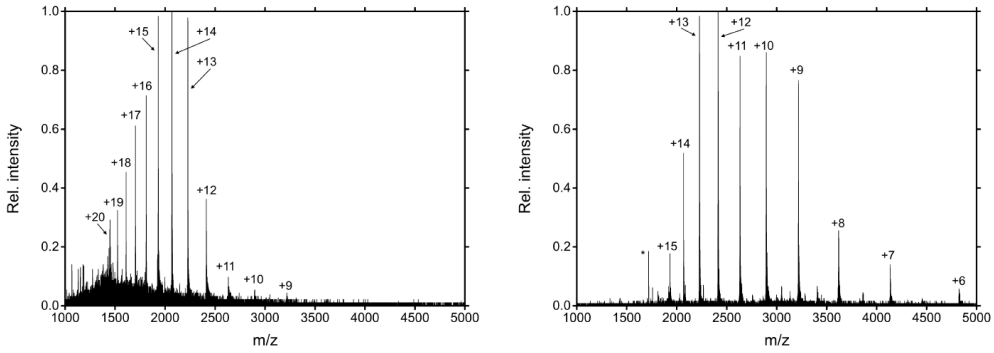

Figure 12: **Comparison of mass spectra with and without charge reduction.** *On the left, the mass spectrum without charge reduction shows multiply charged Green Fluorescent Proteins (GFP) with a mass of* 17 kDa*. The cations have between 9 and 20 charges. With the corona discharge activated, the charge states reduce to between 14 and 6 charges - which is shown on the right.*

In preliminary studies, we used N_2 as ionisation gas and combined it with vapours from water, ethanol and formic acid. Depending on the ionisation mode, this should reduce additional peaks that appear due to the addition of oxygen and nitrogen atoms to the studied molecular beam [68]. But, in later experiments with photocleavable tagged insulin the background air of the laboratory turned out to be a low-maintenance option that produced a beam of stable singly charged insulin.

4.5 Alternative Charge Reduction Schemes

We demonstrated corona discharge reduction of Insulin in our experiments, but for bigger proteins and other biomolecules alternative schemes exist. Since the invention of soft ionisation mass spectrometry, several different possibilities have been developed to obtain low-charged analytes. In this section, I will discuss the most used techniques and recent developments in the field.

A similar approach to corona discharge is charge reduction by α-particle sources, which are commercially available and easy to implement. Radioactive components such as polonium emit He^4 nuclei because of their inherent nuclear instability. These nuclei – also called α-particles - are positively charged and can charge reduce molecular anions through collisions. In the setup described above, it is possible to exchange the ionisation chamber with the polonium source and use the same neutralisation

chamber where analytes and α-particles interact. The opening area between the radioactive source and the neutralisation chamber then determines the charge reduction efficiency [68]. In comparison to corona discharge, the α-particle source is more efficient in reducing the charge states of insulin. However, it is so efficient that with increasing source area most molecules get neutralised. In absolute numbers, the polonium source creates less singly charged proteins. Another crucial disadvantage is that the positive charge of α-particles makes the charge reduction mechanism only feasible for molecular anions.

Manipulation of charge states of gas-phase ions can also be achieved as the byproduct of electron transfer dissociation (ETD). This process is a standard procedure in biochemical analysis to decipher complex mass spectra by fragmenting high-mass biopolymers [66]. In ETD-MS, radical anions are stored in an ion trap and transfer electrons to the analyte cations via collisions. By changing the acceleration potential of the molecular beam, dissociation can be minimised and charge reduction becomes the dominant process. This method produced singly charged haemoglobin with a mass of 64 kDa and is also promising for bigger proteins. But the need for an ion trap and the limitation to molecular cations prevented us from applying this technique to our experiment.

A novel charge reduction tool utilises the combination of two electrospray sources of different polarity [71]. In a single chamber, both sprays aim at the same mass spectrometer inlet and enable singly charged protein cations. The negative electrospray consists of small singly charged anions of methanol. A metallic grid decouples the two sprays and stabilises the protein beam. By varying the distance between the opposite-polarity sprays, it is possible to control the efficiency of charge reduction. Even though this method has been recently reported for the first time, it was already reported to produce singly charged high-mass proteins such as immunoglobulin G with 150 kDa and could, in principle, be implemented in our setup.

As discussed in the following chapter, we demonstrated charge reduction of peptides and proteins in vacuum with UV laser radiation [72]. Electron photodetachment experiments showed that photo-excitation of proteins relax by electron emission [73]. But because lower charge states require higher laser energies this approach is limited to multiple charges in tabletop UV laser setups. We have developed a process that enables charge neutralisation of proteins in such settings: photocleavable tags.

5 Photocleavable Tags and Peptides

In my project, I studied different methods of biomolecule charge reduction and neutralisation to develop a novel source for quantum interferometry of proteins. The goal was to identify a process that creates a cold, slow and collimated beams of neutral insulin. Our main focus was the design and optimisation of photocleavable tags (PCT) that we attached to different peptides and proteins. This photofragmentation mechanism allows us to control the charge state of compounds in vacuum after soft desorption and ionisation by electrospray. As a result, we were able to photocleave singly charged insulin in the gas phase and create a molecule beam of electrically neutral proteins.

5.1 Experimental Setup

Our experiments were conducted on a modified *Waters Q-TOF* - a commercial Electrospray Ionisation Mass Spectrometer (ESI-MS) that enables us to analyse solutions of biomolecules and control molecular beams in vacuum. The different steps of our experimental setup are sketched in **figure 13**. First, a $250\,\mu$L syringe sprays the analyte solution into the machine at a stable rate between $2-10\,\mu\mathrm{L/min}$. The solution disperses at the outlet of a $500\,\mu$m capillary set to a voltage of 2-4 kV. A nebuliser gas flow of 20-100 $\mathrm{L/hr}$ evaporates the solvent in the liquid droplets. After several steps of coulomb fission and further solvent evaporation, isolated gas-phase ions get accelerated into the corona discharge chamber. In the chamber, ions with opposite polarity charge reduce the biomolecular ions by collision. The process creates a sufficient amount of singly charged particles which can be mass selected by the subsequent mass filter.

When the molecules enter the vacuum chamber, we collimate the beam by a stack of ring electrodes. Then we mass select specific *m/z* ratios with the following quadrupole mass filter. By controlling the radio frequency voltage applied to the mass filter, we deflect all particles of *m/z* ratios that deviate from the filter setting. Selected particles enter the collision cell in which they collide with argon gas. A cryogenic cooler enables us to change the temperature of the gas molecules and therefore reduce the internal energy of the molecular beam. This process allows us to study the temperature dependence of fragmentation processes. Ultimately, we obtain a mass-selected and charge reduced molecular beam that can be steered and temperature controlled in high vacuum.

Behind the collision cell, molecules enter a hexapole region in which they interact with the counter-propagating laser beam. The absorption of UV photons leads to fragmentation of the photocleavable tag and subsequent separation of biomolecules and the cleaved leaving group.

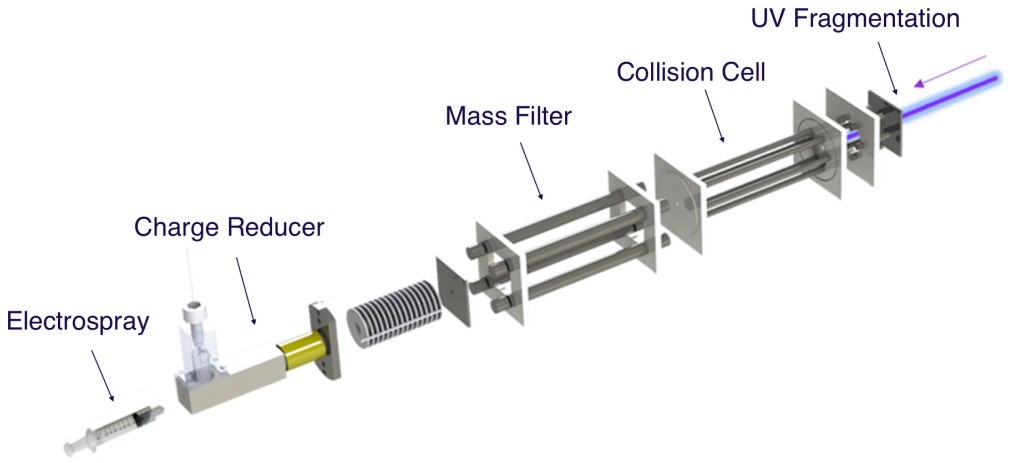

Figure 13: **Setup for charge reduction of photocleavable peptides and proteins.** *Molecules in solution are sprayed through a electrically charged capillary forming a Taylor cone. After acceleration by an electric field the liquid droplets disperse due to a nebuliser gas. Molecular ions enter the vacuum chamber through the charge reducer. There, the particles collide with ions of opposite polarity and get charge reduced. Then, we select a specific m/z ratio by a quadrupole mass filter and cool the molecular beam in a temperature-controlled collision cell. A counter-propagating UV laser beam illuminates the molecules at the following hexapole and photocleaves the tags to neutralise the ions.*

After these stages, we detect charged particles in a Time-of-Flight Mass Spectrometer (TOF-MS) in a V trajectory [74]. In this configuration, molecules get repelled by a pulsed electric field into a reflectron that consists of a high voltage gradient of opposite polarity to the repeller. The gradient, created by a stack of ring electrodes, reduces the kinetic energy distribution of the ions and thereby increases mass resolution additionally to the longer flight path in the V configuration [75]. The ion trajectory is depicted in **figure 14**.

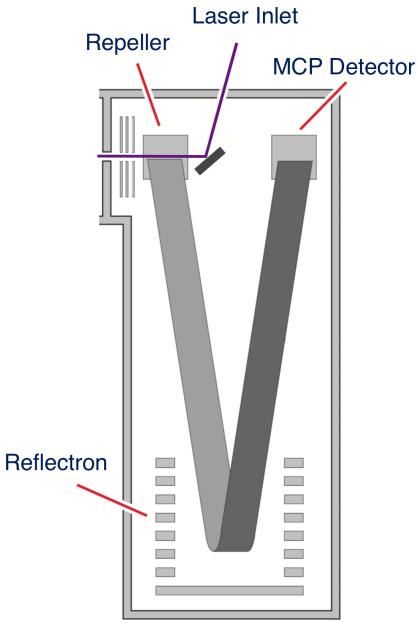

Figure 14: **Molecule detection with time-of-flight mass spectrometry.** *Molecular ions enter the time-of-flight chamber through the opening to the left and accelerate downwards due to the pulsed repeller voltage. The reflectron is a stack of ring electrodes that accelerate the ions upwards onto the multi-channel plate detector. On top of the vacuum chamber, we inserted a window as an inlet for the UV laser beam that is reflected into the electrospray chamber where it interacts with the molecules. Adapted from* ***Waters Q-TOF*** *manual [76]*

5.2 Sample Preparation and Electrospray Parameters

Electrospray ionisation disperses molecules dissolved in a liquid into an aerosol. To prepare the sprayed solution, we added $1\,\mathrm{mg}$ of analyte in dry form to $1\,\mathrm{ml}$ of methanol, then $1\,\mathrm{mL}$ of deionised water, and at the end $1\,\mu\mathrm{L}$ ammonia for the positive mode and formic acid in the negative mode. The last step increases or decreases the pH value of the mixture to optimise ionisation efficiency depending on the polarity of the ionisation process. This solution is then sprayed with a flow rate of $2\text{-}10\,\mu\mathrm{L}$ through the electrospray capillary at a voltage of $3.5\,\mathrm{kV}$ in the positive and $-3\,\mathrm{kV}$ in the negative detection mode.

The entrance cone to the vacuum chamber produced optimal throughput at $35\,\mathrm{V}$ and the MCP voltage was set to the maximum of $2.4\,\mathrm{kV}$. The TOF-MS acceleration

voltage was set to $9.1\,\mathrm{kV}$ for all measurements with its polarity depending on the detection mode. We used nitrogen as cone gas at a flow of $22\,\mathrm{L/hr}$ and as nebuliser gas to dissolve aerosol droplets after the capillary at $50\,\mathrm{L/hr}$. The desolvation temperature at the vacuum entrance was set to $140\,^{\circ}\mathrm{C}$ and the source temperature of the capillary to $100\,^{\circ}\mathrm{C}$.

For the UV photofragmentation experiments we used a frequency-quadrupled, pulsed Nd:Yag laser with a wavelength of $266\,\mathrm{nm}$ and a pulse width of $1\,\mathrm{ns}$. The laser beam was aligned collinear and counter-propagating to the molecular beam and had a spot size of $2\,\mathrm{mm}$. The most important measurement parameters for the results discussed in this thesis are collected in table **table 1**.

Table 1: ***Important parameters for the electrospray measurements.*** *RF 1 is the voltage applied to the first collimation radio frequency lens. Laser power and frequency give the strength and repetition rate of the UV laser that interacts with the molecular beam, and the measuring time depends on beam stability and intensity. Molecules with lower count rates were recorded for a longer time to ensure sufficient statistical power.*

	RF 1 (V)	Laser Power (mW)	Laser Frequency (Hz)	Delay (us)	Measuring time (s)
PCT tripeptide	30	94	250	48	120
PCT nonapeptide	30	94	250	48	120
PCT dodekapeptide	30	94	250	48	120
pos cPCT tripeptide	10	94	250	80	240
neg cPCT tripeptide	10	94	250	98	120
pos cPCT insulin	100	560	1000	100	480
neg cPCT insulin	100	560	1000	100	120

5.3 Neutral Photocleavable Tags

Our source mechanism produces high-intensity beams of singly charged peptides and proteins but to create a neutral beam of biomolecules we had to find a way to remove the last charge on the specimens in vacuum. This was achieved by tagging the particles with a molecule chain that fragments under UV irradiation. The so-called photocleavable tag (PCT) enables us to control the charge state in the gas phase and the first version of it is shown in **figure 15**.

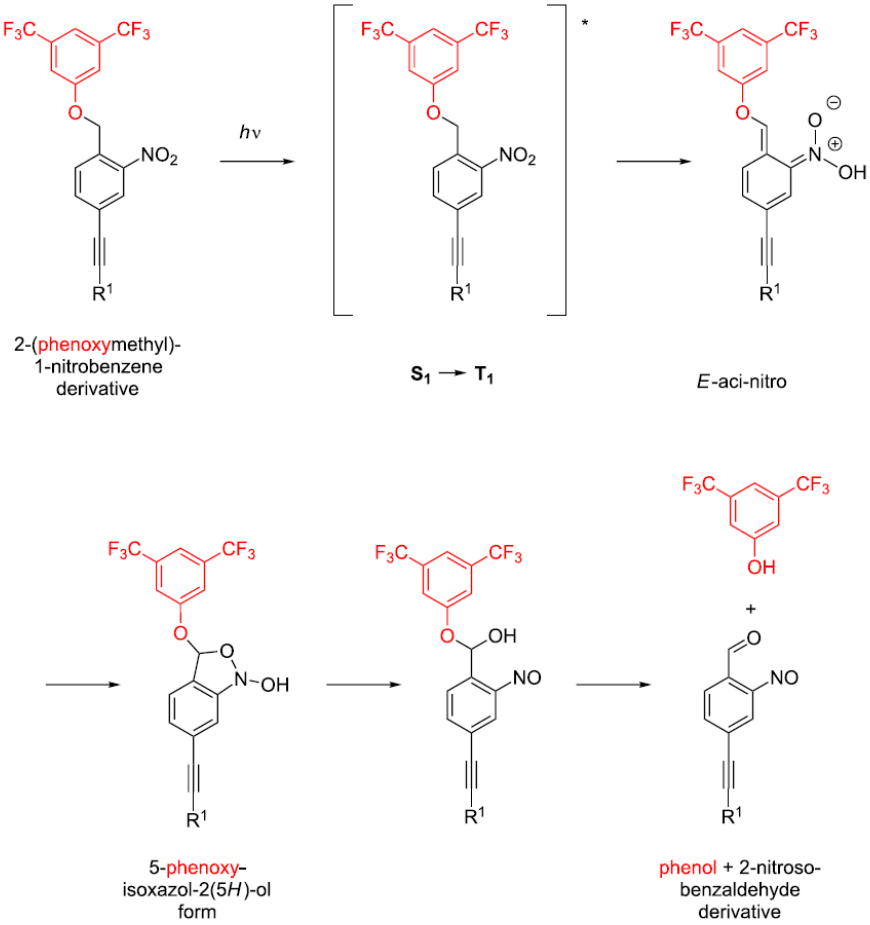

Figure 15: **Chemical structure of photocleavable tags and intermediary steps of the photocleavage pathway in solution.** *The photocleavable tag absorbs UV photons and enters a triplet state T_1. Hydrogen transfer leads into the E-aci-nitro form. After formation of a cyclic isoxazol, the molecule fragments into a phenol subunit and 2-nitrosobenzaldehyde. Adapted from [22]*

The photocleavable tag is attached to the molecule at position R^1. This tag is designed as a universal building block that connects to a broad range of biomolecules via easy-to-implement click chemistry reactions [22]. This class of reactions allow the fast and effective attachment of small reporter molecules to bigger biological structures in solution [77]. We have chosen a 2-(phenoxymethyl)-1-nitrobenzene motif because its photochemical reaction does not depend on background molecules from solvents but only on intramolecular exchange. This is necessary to ensure that our chosen mechanism is applicable to molecular beams in vacuum conditions where no solvent

molecules are present.

Photocleavage in solution consists of the absorption of UV photons, which excite the molecule into its singlet state. By intersystem crossing, the singlet state decays into its triplet state and in the next step, the transfer of hydrogen leads to the E-aci-nitro form of the molecule. This form decays into cyclic isoxazol, shown in step 4 of **figure 15**. In the next step, the hydrogen moves closer to the fragile oxygen bond and because of molecular instability a phenol fragment and 2-nitrosobenzaldehyde arise as end products.

The PCTs were designed in such a way that UV irradiation breaks the oxygen bond between the photolinker and the leaving group. While studying the mechanism of photocleavage in solution we observed the fragments corresponding to the expected reaction. The continuous irradiation of molecules with light from a UV lamp lead to increasing signal of the phenol subunit. This provided evidence that our design of PCTs would enable the same mechanism in vacuum. But, it was still possible that missing solvent background molecules would lead to different behaviour after UV photon absorption.

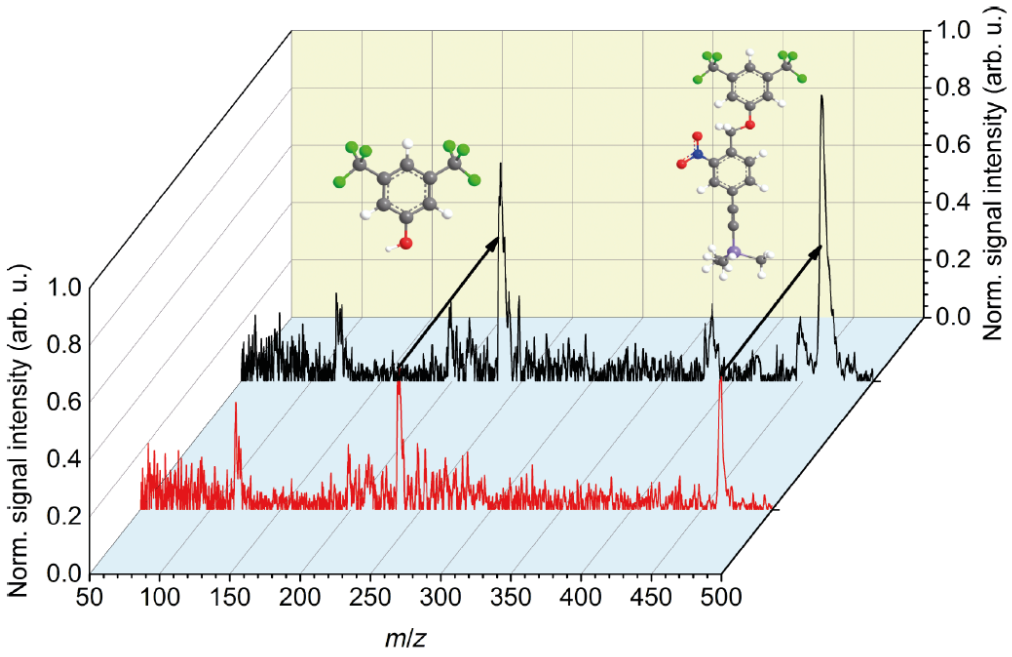

Figure 16: ***Mass spectrum of photocleavable tags under UV radiation.*** *In the black curve, the intact PC molecule appears at a mass-to-charge ratio of* $461\,\mathrm{m/z}$*. Additionally, the photocleaved group can be seen at* $229\,\mathrm{m/z}$*. The red curve consists of data after UV laser interaction with the molecular beam. The ratio between intact and photocleaved signal changes with UV radiation. These results were part of preliminary studies that were conducted on molecular beam machine before we employed the ESI-MS setup. Adapted from [22].*

In figure **figure 16**, we show the mass spectrum of PCTs isolated in the gas phase. The results were recorded during preliminary studies with the first generation of synthesised molecules in a molecular beam machine and after thermal desorption of molecules with an infrared laser. Further details of the setup are discussed in our article by Sezer and colleagues [22]. Even though, we were not able to demonstrate conclusive fragmentation of the designated molecule bond we detected the particles at the correct mass and observed a significant effect of UV laser light on the photocleavable molecules. Fragments from the source mechanism hindered the quantitative analysis of the photocleavage process. To overcome this limitation, we switched to the electrospray ionisation setup that allows mass selection before UV irradiation and therefore quantitative analysis of fragmentation yield.

In preliminary studies of PCTs in vacuum, we detected intact molecules at the cor-

rect mass and observed a significant effect of UV radiation on the molecular tags [22]. To extend our study of the photocleavage mechanism in the gas phase, we connected the tags to a range of model peptides and tested the modified biomolecules under soft desorption of electrospray ionisation. The studied amino acid chains ranged from three to twelve building blocks and allowed us to compare the behaviour of tagged particles with different length and mass.

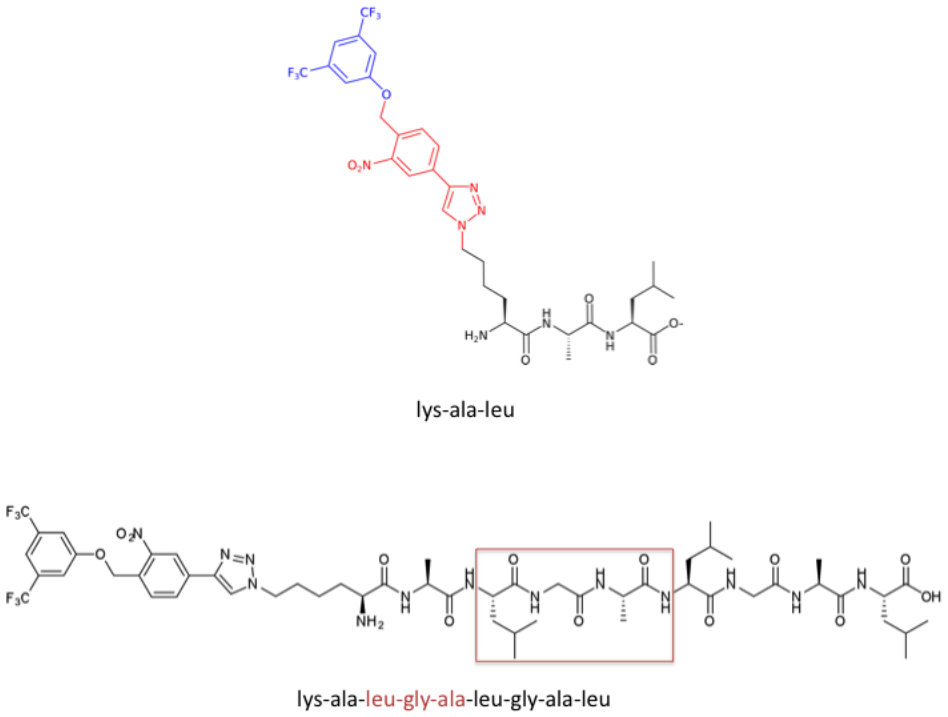

Figure 17: **Structure of photocleavable tagged peptides.** *The top panel shows the chemical structure of the photocleavable tagged tripeptide. The blue part represents the leaving group which separates from the biomolecule, the red part consists of the photolinker which is used to connect tags to different molecules and the three amino acids - the tripeptide - are depicted in black. The bottom panel shows the structure of a nonapeptide - made out of nine amino acids. The sequence consists of the same start and end molecules - Lysine-Alanine and Leucine respectively - with a repeating motif of Leucine-Glutamine-Alanine in-between. This motif is highlighted in the red box.*

When irradiated with the UV laser, we observe a characteristic fragmentation pattern that is depicted in **figure 18**. The particles in solution already produce charged leaving group signal and other fragments. With mass selection, we clean the signal

to produce a beam of intact photocleavable peptides at a mass of 744 Da. Afterwards, this beam interacts with UV photons and produces fragments of phenolate which can be detected at 229 Da. We expect the residual molecule to be in a dipolar state, where a negative charge sits on the peptide chain and a positive charge arises on the fragmentation site. Because the dipolar state does not interact electrically with our setup, we are not able to detect the remainder of the reaction in the mass spectrometer.

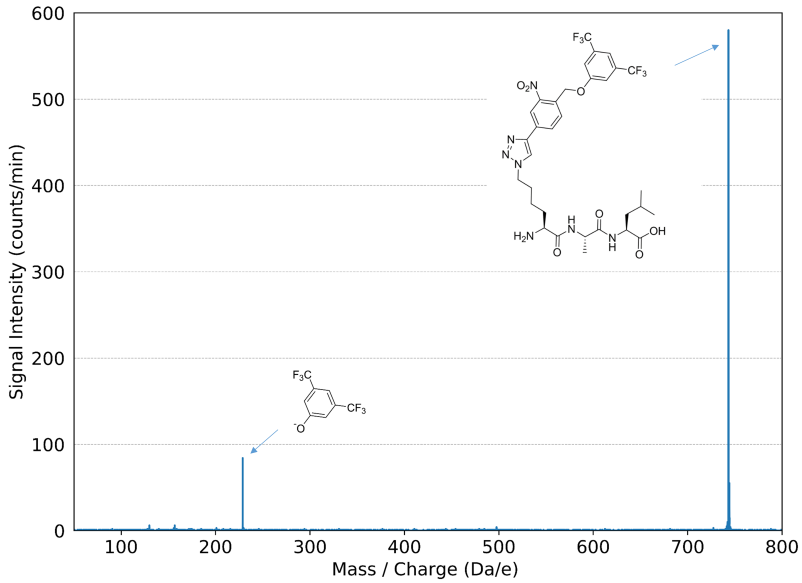

Figure 18: **Mass spectrum of photocleaved peptides.** *Negative electrospray ionisation of photocleavable tripeptides produces intact and singly charged molecules at a mass of* 744 Da*. After absorption of UV photons, the tagged molecule fragments into a neutral tripeptide and a negative phenolate which is detected in our time-of-flight mass spectrometer at* 229 Da*.*

To further understand the involved photofragmentation processes, we studied photodepletion - the reduction of the main peak signal in relation to UV laser power. By comparing the photodepletion efficiency at varying laser power, we can differentiate between single- and multi-photon depletion processes. S_0 denotes the initial ion signal and S is the reduced signal when irradiated by the laser. If we assume kinetic rate equations, the photodepletion efficiency $1 - S/S_0$ [78] is given by

$$1 - \frac{S}{S_0} = 1 - \alpha + \alpha \left(1 + \gamma \sigma F\right) e^{-\sigma F}. \tag{12}$$

From this equation, we see that the photodepletion efficiency depends on the spatio-temporal overlap α of molecular beam and laser, the fraction of two-photon processes γ, the photodepletion cross section σ, and the varying laser fluence F [25]. Here we assume that the overlap α is equal for the first and subsequent photon absorption.

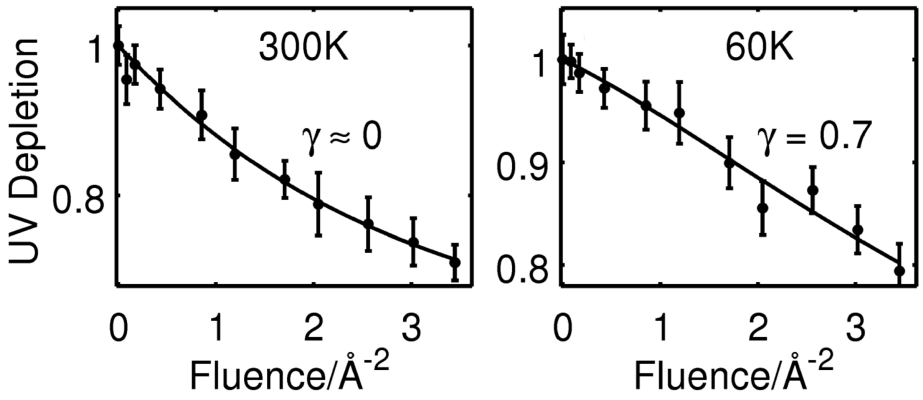

Figure 19: **Photodepletion depending on laser fluence at different temperatures.** *The left plot shows the depletion efficiency at room temperature of 300 K. In comparison, the right plot presents the depletion when the molecular beam is cooled down to 60 K. The solid lines represent the fit by kinetic rate equations and γ gives the ratio of two-photon processes involved in the depletion. Adapted from [25]*

Interestingly, we observed different processes for photodepletion at 300 K and 60 K. As shown in **figure 19**, the fit at room temperature corresponds to a single-photon process that exhibits exponential decay. In contrast, the depletion curve at 60 K can be described by $\gamma = 0.7$ or 70 % two-photon processes. Therefore, we conclude that the molecular temperature changes the photodepletion behaviour of PCT Peptides. A lower internal temperature decreases the likelihood of photocleavage processes because more photons are needed to overcome the bond energy and trigger the fragmentation pathway.

When we compared the fragmentation yields of the phenolate group for different peptides, we made another interesting observation. Contrary to our expectations, longer peptides showed a significant decrease in fragmentation yield for the leaving group. With the longest peptide of 12 amino acids showing no phenolate signal in our experiments at all. In **figure 20**, we plot the relation of the peptide length to

the fragmentation yield. Surprisingly, the expected fragment at 229 m/z is substituted by another fragment that is higher in mass. Further analysis showed that the newly discovered subgroups correspond to the peptide chain with a missing PCT and an additional Hydrogen or [M - 230 Da]. This implies that the charge stays on the peptide and not as intended on the cleaved fragment. Another prevalent signal in this spectrum consists of the latter molecule which loses an additional oxygen of 16 Da.

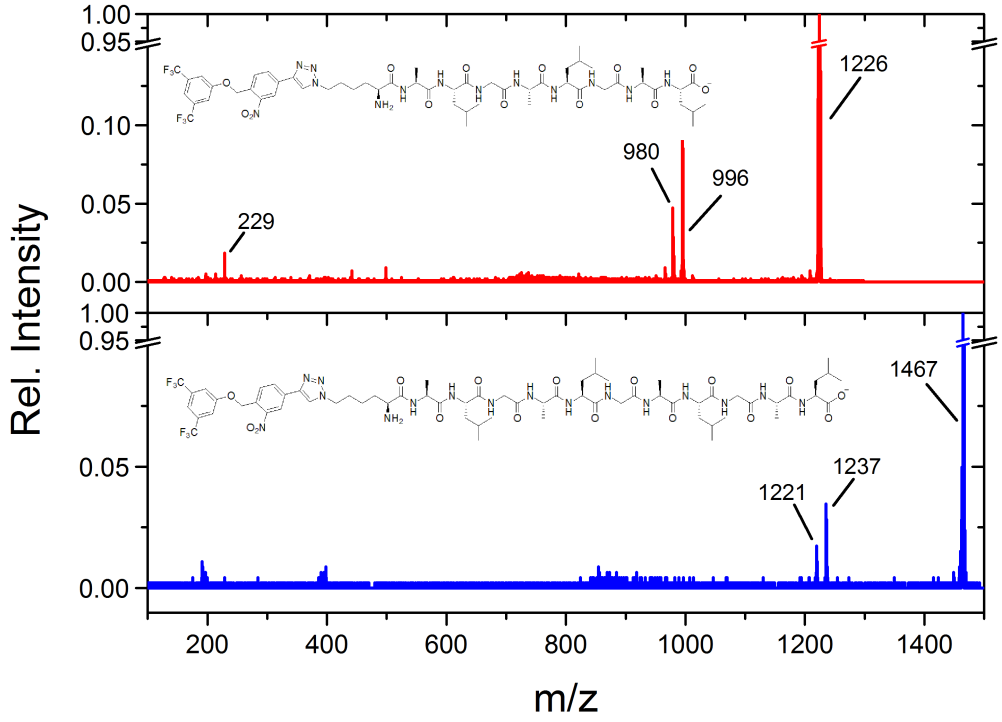

Figure 20: **Fragmentation yield of longer peptide chains.** *The upper panel shows the fragmentation pattern of a nonapeptide chain with the expected leaving group at* 229 Da*. This peak is already surpassed by a proton transfer fragmentation pathway that produces charged peptide chains at* 996 Da *and* 980 Da*. The bottom panel presents the mass spectrum of a dodekapeptide or twelve-peptide chain. The leaving group is absent and only the proton transfer fragments can be detected at* 1221 Da *and* 1237 Da*.*

From this observation, we conclude that the photocleavage mechanism changes with increasing length of the polypeptide. It is therefore impossible to charge reduce longer peptides with the presented molecular tag. Because of our experimental re-

sults, we redesigned the PCTs to carry a fixed charge at the phenol subgroup. This lead to the synthesis of charged Photocleavable Tags (cPCT) which are discussed in the next section.

5.4 Charged Photocleavable Tags

In comparison to the original PCT, the second generation of molecular tags was synthesised with a different goal in mind. The old tags possessed a strong electronegative end that was supposed to take up an electron after photocleaving. In contrast, the new tags have a fixed charge on the removable fragment - or leaving group - which leads to charge reduction independent of the fragmentation pathway. Therefore, we call them charged Photocleavable Tags (cPCT). We synthesised two different designs for extraction of a negative or positive fragment to enable charge reduction in both polarity modes.

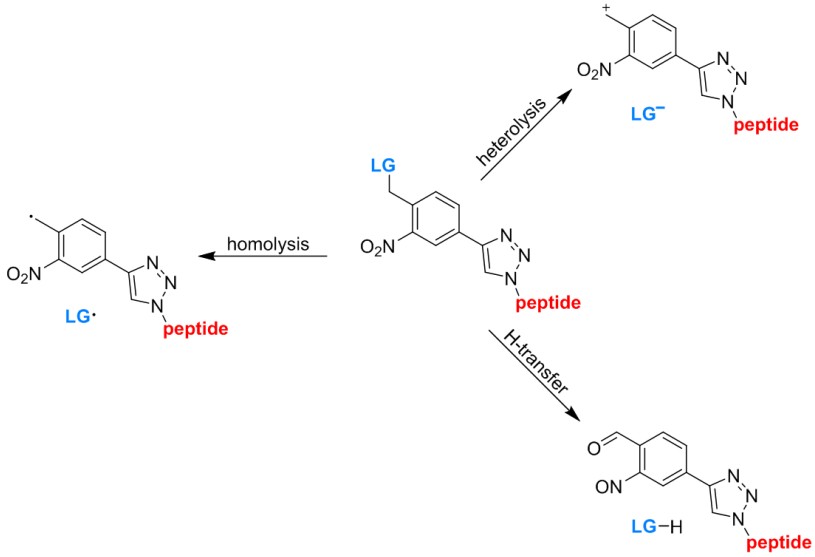

Figure 21: **Fragmentation pathways of photocleavable peptides.** *Heterolytic fragmentation consists of breaking the photocleavage bond and subsequent forming of a phenolate as negative leaving group. This process was observed for small PCT peptides. Proton transfer fragmentation leads to an additional proton on the leaving group and no charge reduction. It was observed for longer PCT peptides and cPCT peptides. Another fragmentation pathway was only present with cPCT: Homolytic fragmentation creates a radical leaving group and peptide. Because of the stabilised charge on the leaving group, either homolysis or heterolysis enable charge reduction of biomolecules. Adapted from [79]*

As observed in studies of neutral PCTs, there are different fragmentation pathways involved in the photocleavage process. Depending on peptide length, we detected signals in the mass spectrum that correspond to different fragments. The short PCT peptides undergo heterolytic photocleavage, where the removed leaving group takes up both electrons of the broken covalent bond. This leads to a dipolar neutral peptide and a negatively charged leaving group. In contrast, the fragmentation of long PCT peptides takes more steps and consists of a jump of oxygen atoms to the broken bond and proton transfer to the leaving group. In this case, no charge reduction takes place and the leaving group is heavier by 1 Da. In **figure 21**, the different fragmentation pathways are sketched.

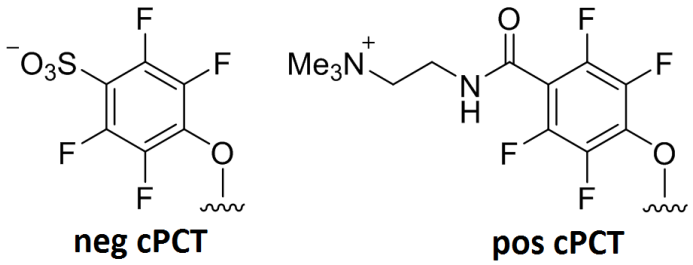

Figure 22: **Chemical structure of charged PCT peptides.** *The neg cPCT has a stabilised negative charge on the sulphur trioxide SO_3 and the pos cPCT consists of an additional chain that stabilises a positive charge on the trimethylamine Me_3N. The wave on the bottom right represents the connection to the photolinker and peptide.*

However, missing charge reduction under proton transfer fragmentation is a problem for designing a universal PCT for charge state control in vacuum. We therefore kept the general composition of photocleavable molecules and adapted the leaving group to carry a stable charge that allows for charge reduction with different fragmentation pathways. The chemical structure of the new cPCTs is depicted in figure **figure 22**. To test the new design, we again attached the cPCT to peptide chains of different length.

The mass spectrum in **figure 23** consists of an intact molecule signal of negative cPCT tripeptides at 761 Da and positive cPCT tripeptides at 810 Da. Additionally, the absorption of UV photons leads to fragments corresponding to the negative leaving group at 244 Da and positive leaving group at 291 Da.

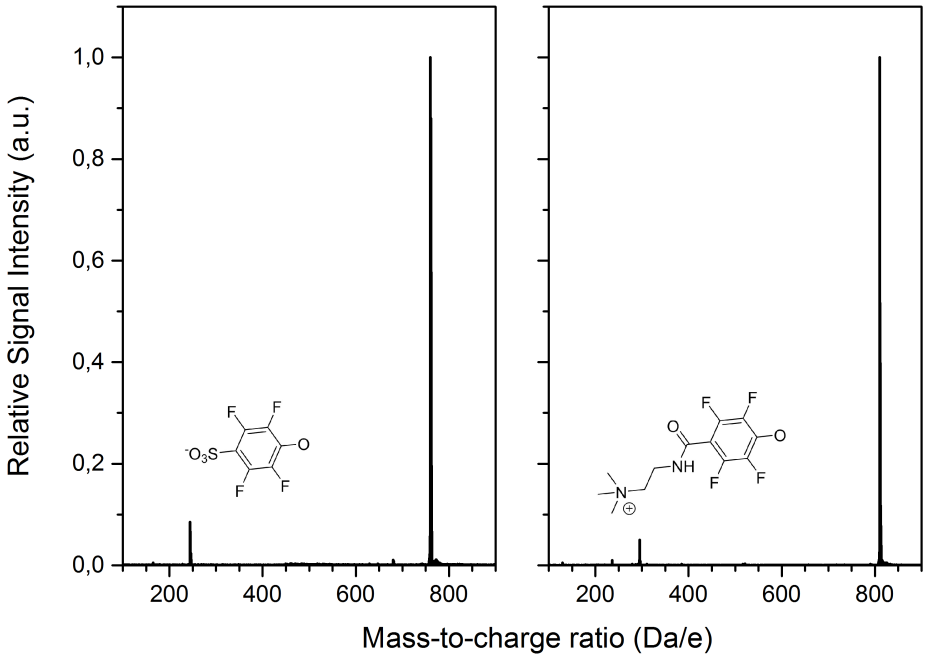

Figure 23: **Mass Spectrum of charged photocleavable peptides after UV irradiation.** *On the left, we show the spectrum of negative cPCT tripeptide after absorption of UV photons. The highest peak corresponds to the intact molecule at* 761 Da *and the second highest peak consists of the photocleaved leaving group at* 244 Da*. On the right, the positive cPCT spectrum is plotted with the intact molecule appearing at* 800 Da *and the leaving group at* 291 Da*. Before the laser interaction, the beam is mass selected for the intact complex and therefore all fragments are due to absorption of UV photons.*

This presents indirect evidence of the successful charge reduction of peptides, but because we are not able to detect neutral particles in our mass spectrometer we do not know if the biomolecules stay intact. It could also be the case that the peptides fragment further into smaller components after photocleaving.

Luckily, the electrospray source produces additional doubly charged cPCT peptides. This enabled us to charge reduce our target molecules from two to one charges and detect both the leaving group and the whole photocleaved peptide. Because we detected photocleavage fragments for both the negative and positive cPCT, we applied this strategy to our target of interest: the small protein insulin. With higher mass and complexity - 1000 Da of the longest peptide compared to 6000 Da of insulin - it

was not clear if this cPCT also charge reduces proteins. We attached three cPCT of both polarities to insulin and I present the results in the next section.

5.5 Neutralisation of Insulin

After preliminary studies on peptides, we planned to attach the optimised cPCTs to a small model protein. In our experiments, we tagged insulin with three tags and observed the first charge neutralisation of a protein in the gas phase. This was achieved in an electrospray mass spectrometer with a coupled $266\,\mathrm{nm}$ laser beam and the corona discharge chamber as a preceding charge reducer.

As sketched in figure **figure 24**, insulin consists of 51 amino acids arranged in two side chains connected by two disulphide bridges. Three PCTs are connected to the insulin at the N-termini amino acids, namely glycine and phenylalanine, and an off-centre lysine on the second chain. Four tyrosine and three phenylalanine residues of natural insulin and the PCTs can absorb the UV photons. But adding up the extinction coefficient of the seven amino acids in the protein amounts to $\epsilon \approx 4200\,\mathrm{M^{-1}cm^{-1}}$, which is approximately five times lower than the combined extinction coefficient of the PCTs $\epsilon \approx 20\,000\,\mathrm{M^{-1}cm^{-1}}$ [80]. To test the photocleavage mechanism, we irradiated multiply charged insulin ions with UV laser pulses.

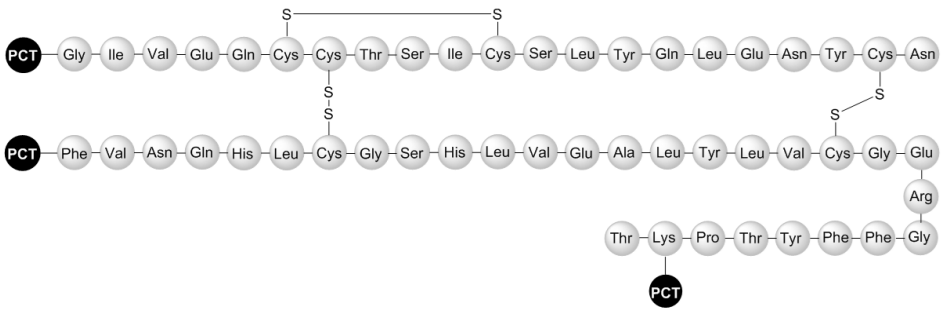

Figure 24: **Amino acid sequence of tagged insulin.** *The cPCTs are connected to glycine of the first chain and phenylalanine and lysine of the second chain. The chains of the protein are connected by two disulphide bridges.*

Our first results demonstrate controlled charge reduction of a 6-times charged insulin anion by photocleavage. **Figure 25** compares the detected spectra with and without UV irradiation. We were able to record the negatively charged leaving group

and the charge reduced photocleaved insulin simultaneously. Additionally, we detected charge reduction by electron detachment of proteins. For highly charged states, we even observed photocleavage of two leaving groups and additionally mixtures of electron detachment and photocleavage.

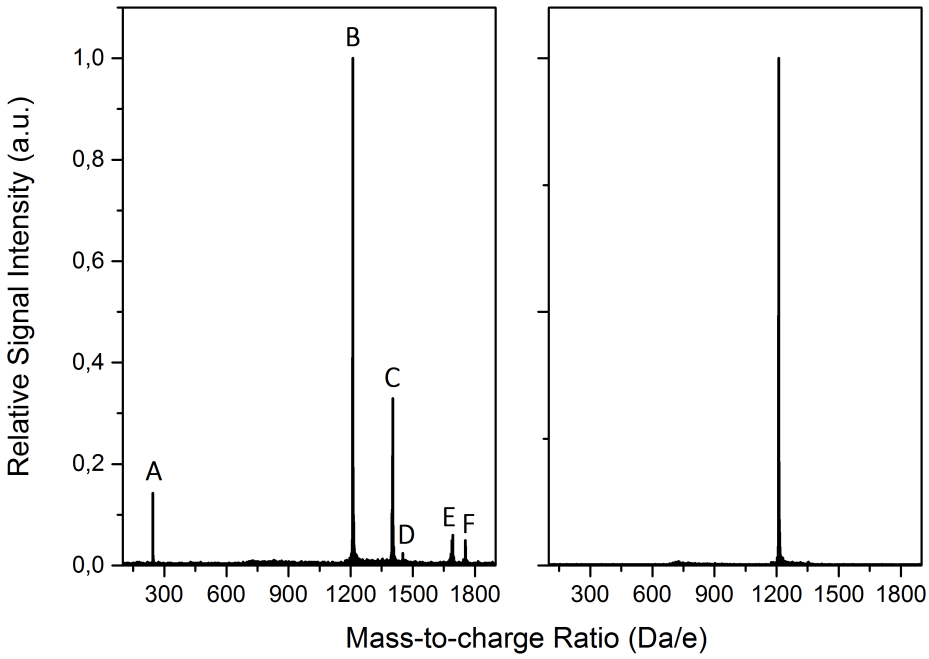

Figure 25: **Charge reduction of cPCT insulin by photocleavage.** *On the right we show the mass spectrum without laser influence and on the left the resulting photofragments from UV laser radiation can be seen.* ***A*** *corresponds to the signal from the cPCT leaving group [LG]* $^{1-}$*,* ***B*** *is the 6-times charged cPCT insulin signal [Ins]* $^{6-}$*,* ***C*** *shows the 5-times charged cPCT insulin after the loss of a leaving group [Ins - LG]* $^{5-}$*,* ***D*** *is the charge reduced Insulin after electron detachment [Ins - e]* $^{5-}$*,* ***E*** *corresponds to a doubly photocleaved protein [Ins - 2LG]* $^{4-}$*, and* ***F*** *shows the low probability of concurrent photocleavage and electron detachment [Ins - LG - e]* $^{4-}$*.*

After observing charge reduction of modified insulin, we tested photoneutralisation by creating a beam of singly charged proteins with corona discharge. The molecules were reduced to the singly charged state in our corona discharge chamber and we subsequently selected singly charged specimen with mass filtering. The mass-selected molecular beam of singly charged cPCT insulin is afterwards exposed

to UV radiation and the fragments are detected in TOF-MS. The resulting signal of photocleaved proteins is plotted in **figure 26**. Here, we present the first evidence for successful photoneutralisation of insulin.

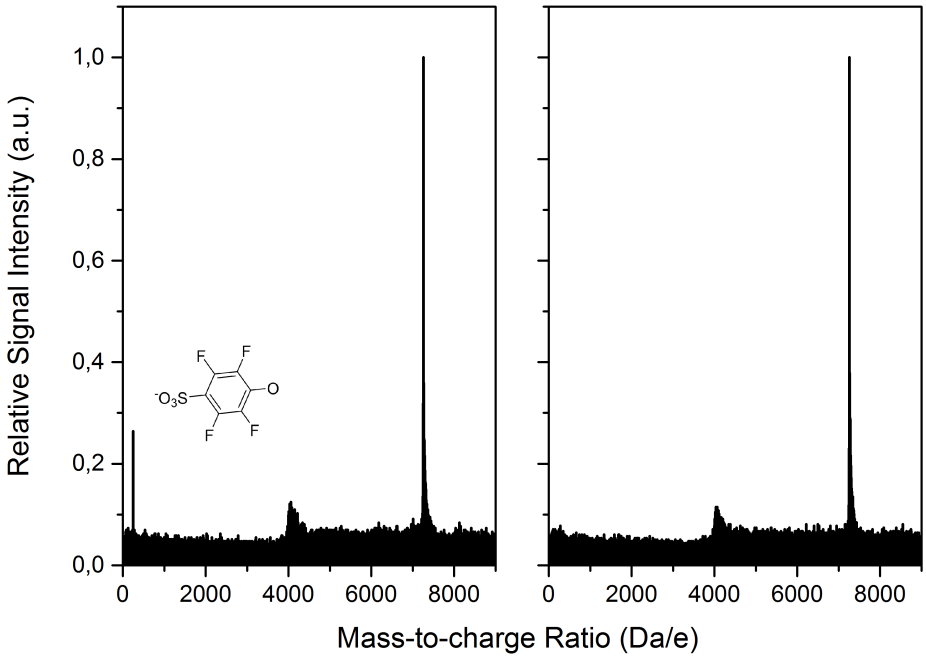

Figure 26: **Neutralisation of cPCT modified insulin in the gas phase.** *After charge reduction in a corona discharge chamber, we mass select the singly charged cPCT insulin. This protein beam interacts with a UV laser and photocleaves thereupon creating negatively charged leaving groups. On the left, we show the photocleavage signal after UV absorption with the leaving group at* 244 Da *and on the right, we plot the signal without laser interaction. Because of low signal intensities of singly charged insulin the noise floor is significantly higher than in previous measurements.*

Through detection of the leaving group at the right mass, we have indirect evidence that UV radiation leads to controlled neutralisation of proteins. Previous studies with multiply charged insulin also showed that insulin stays intact after charge reduction and could, therefore, be used as a beam source for protein interferometry.

In additional measurements, we recorded the fragmentation yield depending on the charge state of negative cPCT insulin. The comparison of the detected leaving group, the charge reduced protein, and the depletion efficiency are plotted in **27**. The

fragmentation yield, depletion efficiency and protein counts are not consistent and appear to peak at a medium charge state. Because of variable detection efficiency's for different mass-to-charge ratios, we assume that these numbers are not representative for the actual number of fragments in the beam. If we would be able to detect all fragments created in our ESI-MS setup, we would expect a direct correspondence between photodepletion, leaving group signal and charge reduction yield. To further study this hypothesis, we could extend our setup with an ion trap that enables the detection of all fragments.

The only other observed charge reduction channel included electron detachment of highly charged insulin, but higher charge states did neither show maximum charge reduction nor maximum leaving group yield. Additionally, the charge reduction yield dropped significantly for lower charge states while the leaving group yield remained present. Notwithstanding, the observed vanishing of electron detachment is consistent with previous studies on native insulin from Brunet and colleagues [72]. In conclusion, our results indicate clearly that photocleavage is the dominant process for lower charge states of cPCT insulin.

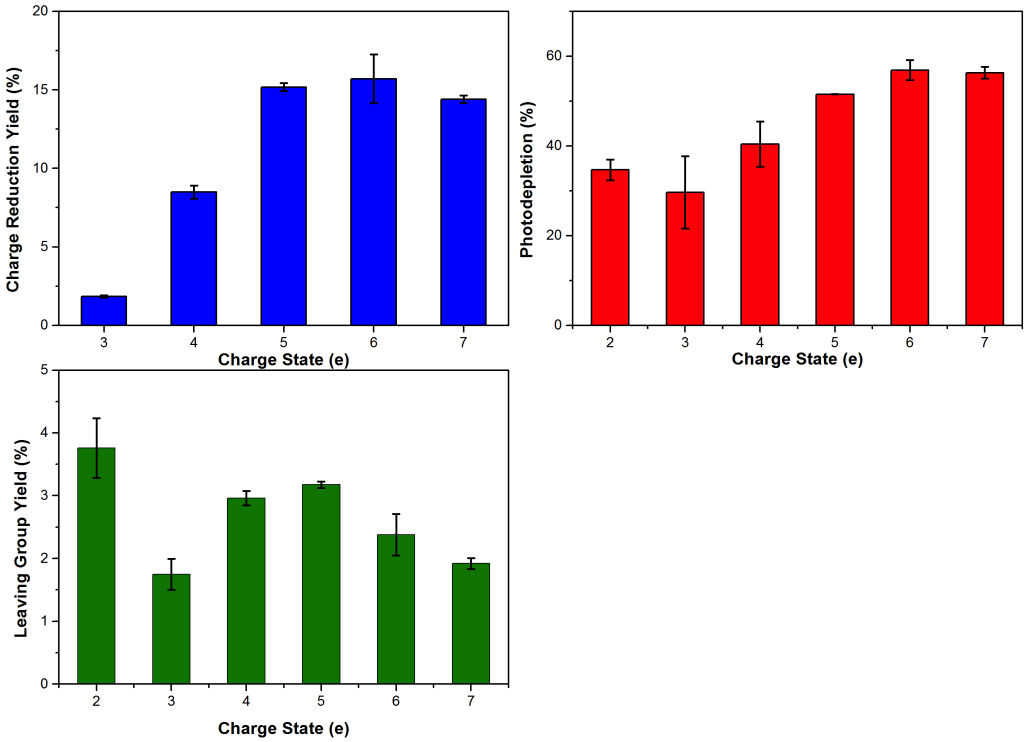

Figure 27: **Yield comparison for negative cPCT insulin.** *In **A**, we show the yield of charge reduced proteins relative to the intact cPCT insulin signal. In **B**, we plot the signal reduction induced by the UV laser as photodepletion percentage. And in **C** we give the relation of leaving group signal to intact insulin. The error bars are calculated from the signal fluctuation over time.*

We also tested the photoneutralisation of single positively charged cPCT insulin but due to beam stability issues, the interpretation of our results is not conclusive. The comparison of photodepletion, charge reduction and leaving group yield is plotted in **figure 28** and overall reflects lower yields and higher error bars in comparison to negative cPCT insulin.

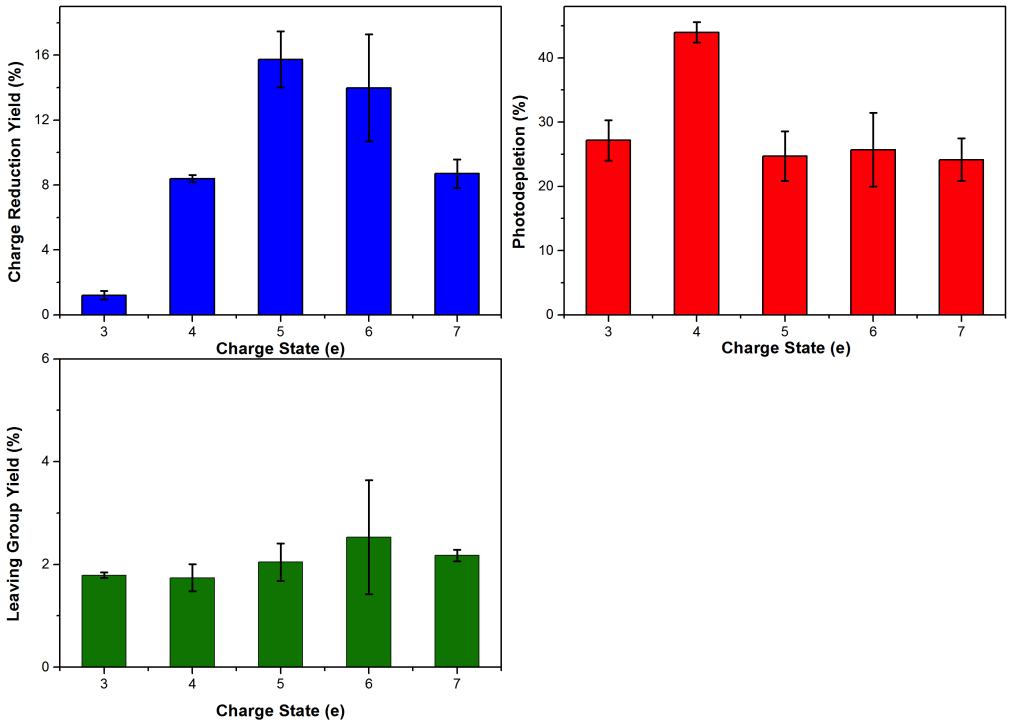

Figure 28: **Yield comparison for positive cPCT insulin.** *In **A**, we show the yield of charge reduced proteins relative to the intact cPCT insulin signal. In **B**, we plot the signal reduction induced by the UV laser as photodepletion percentage. And in **C** we give the relation of detected leaving group counts to the signal of intact insulin.*

The fragmentation yield, depletion efficiency and protein counts peak at different charge states and a comparison is hindered due to inherent experimental uncertainties and the aforementioned limitation of not detecting all produced fragments. Therefore, we conclude that further studies with cleaner synthesised material and higher detection efficiency are required to understand the photocleavage mechanism of positive cPCT insulin. Nonetheless, we demonstrated the first successful charge reduction by photocleavage of a protein also in positive polarity.

6 Discussion and Outlook

In a series of experiments conducted over three years, we were able to demonstrate charge state control, cooling and focusing of peptide and insulin beams in vacuum. By extending this method into the higher mass range we hope to enable quantum interferometry with complex biomolecules such as different proteins and DNA. We were able to control the particle velocity and focus molecules by guiding the ions in a radio frequency hexapole field down to five volt of acceleration potential. This corresponds to a velocity of $366\,\mathrm{m/s}$ for tagged insulin. The buffer gas cell provides further deceleration. The corona discharge chamber and the use of photocleavable tags allows for the control of the charge state of peptides and proteins down to electrical neutralisation. Our results therefore provide evidence for the successful use of electrospray ionisation and subsequent charge reduction to prepare neutral, cold, and collimated biomolecular beams for a wide range of vacuum experiments in biochemistry and molecular physics. This also opens up the possibility to perform quantum assisted metrology on these essential molecules for life.

The next step of our research includes the application of cPCTs to bigger proteins such as myoglobin which consists of 153 amino acids, with a total mass of $17\,\mathrm{kDa}$. In preliminary experiments, we were able to charge reduce native myoglobin and detect a wide range of charge states in our setup. This first test of higher mass proteins is shown in [figure 29]. Charge reduction by corona discharge and photoneutralisation with presented cPCT modifications could provide a universal source for neutral proteins. Our goal is to bridge the gap of several magnitudes of mass to ionise and control a beam of tobacco mosaic viruses with around $40\,\mathrm{MDa}$ [81]. Our earlier soft desorption experiments did not create intact viruses in the gas phase but electrospray ionisation could overcome these problems [82].

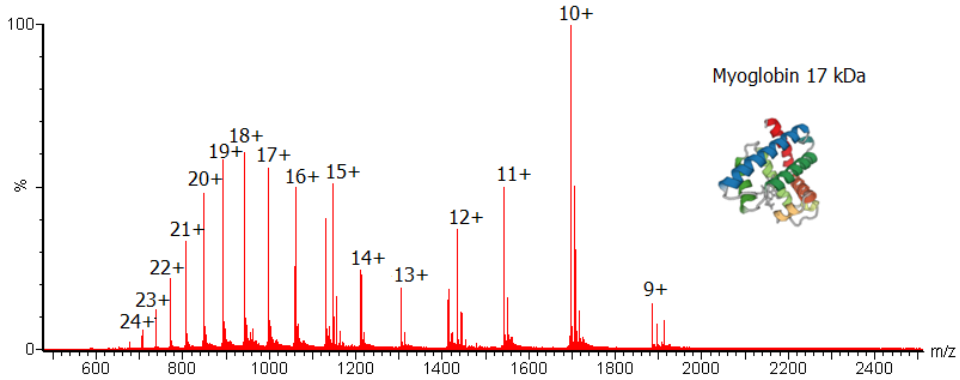

Figure 29: **Electrospray ionisation and detection of myoglobin.** *Native myoglobin shows a wide range of charge states in electrospray setups, but we demonstrated effective charge reduction of these proteins in a corona discharge chamber [69]. Modifying high mass proteins with cPCT could enable a subsequent photoneutralisation by absorption of UV photons in vacuum.*

To increase the photocleavage efficiency for bigger biomolecules, we also plan to extend the vacuum chamber before the particles enter the mass spectrometer. By adding a separate chamber, we would be able to align the laser beam orthogonally to the molecular beam in an optical cavity. This would enable us to use higher laser powers in the ultraviolet and produce a higher rate of neutralised proteins.

Another tagging strategy could improve the low efficiency of neutral molecule detection. Additional fluorescent tags enable the detection of biomolecules in vacuum without the need for post-ionisation - one of the big challenges in mass spectrometry to date [83]. In **figure 30**, I show one of the first candidate molecules to study concurrent photocleavable and fluorescent tags.

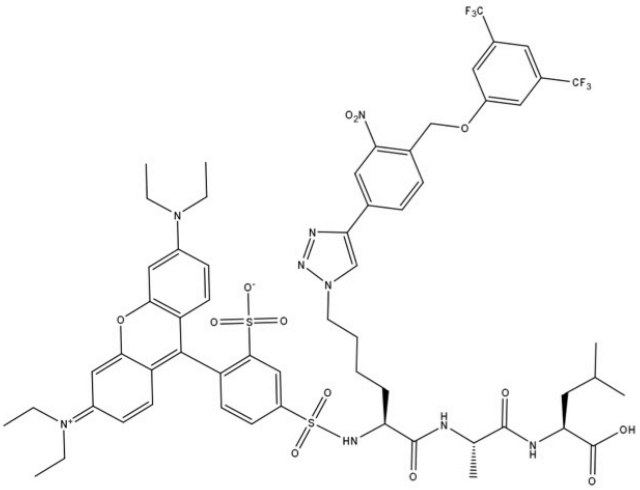

Figure 30: **Chemical structure of flourescent labeled PCT polypeptides.** *Additional to the photocleavable tag, we attached a rhodamine lissamine B which fluoresces in red at around* 600 nm *[84]. This tag could be used to detect a wide range of neutral biomolecules in vacuum.*

In conclusion, we gathered substantial evidence that photoactive molecular tags enable us to overcome many limitations of quantum interferometry and quantum assisted metrology of complex biomolecules. Photocleavable tags have opened many possibilities for charge state control of peptides and proteins in the gas phase and fluorescent tags have the potential to optimise the detection of neutral biological complexes. In this thesis, I provide results that demonstrate why this strategy can be used as a novel beam source for quantum interferometry. The study of proteins and viruses is not only interesting to reach new mass limits in matter-wave experiments and to study optical properties of biomolecules [85], but could also shine a light on how the complexities of life influence mesoscopic behaviour on the edge of classical and quantum physics.

Appendices

A Interpretations of Quantum Interference

In this thesis, I describe the experiments and results without committing to a specific interpretation of the equations of quantum physics. Concepts such as delocalisation, which-path information and collapse of the wave function usually refer to the orthodox interpretation originally developed by Bohr and Heisenberg from 1927 onwards, also referred to as Copenhagen interpretation [86]. Even though this view is usually taught in textbooks as well-defined, there is still an ongoing discussion about its fundamental principles. It has been argued that Bohr and Heisenberg disagreed on many positions such as complementarity [87].

In explaining matter-wave experiments, we often use ambiguous language to connect the counter-intuitive observations to our everyday experience [88]. Statements such as "the particle goes through both slits at once" are not only experimentally unjustified, they also carry a lot of philosophical assumptions that have never been explicit. To understand why it is important to point this out in an experimental master thesis, I will give a short motivation of the discussion concerning the wave function Ψ and its relation to our experimental results.

In his lectures about quantum mechanics, Richard Feynman wrote the following about the electron double-slit experiment [89]:

"Is it true, or is it not true that the electron either goes through hole 1 or it goes through hole 2? The only answer that can be given is that we have found from experiment that there is a certain special way that we have to think in order that we do not get into inconsistencies. What we must say (to avoid making wrong predictions) is the following. If one looks at the holes or, more accurately,if one has a piece of apparatus which is capable of determining whether the electrons go through hole 1 or hole 2, then one can say that it goes either through hole 1 or hole 2. But, when one does not try to tell which way the electron goes, when there is nothing in the experiment to disturb the electrons, then one may not say that an electron goes either through hole 1 or hole 2. If one does say that, and starts to make any deductions from the statement, he will make errors in the analysis. This is the logical tightrope on which we must walk if we wish to describe nature successfully."

Feynman was fully aware of the counter-intuitive concepts of the experiment and

the following section will discuss a few interpretations that give new insights into it.

A.1 Ontology of the wave function

As explained in **Chapter 2**, matter-wave experiments build on the idea that the quantum wave function describes the dynamics of our particles in the interferometer. If we do so, the question arises why we can only indirectly access the wave behaviour of molecules. In the end, we just measure an ensemble of particles at our detector and every additional inquiry about their position leads to decoherence. This exemplifies a couple of open questions in quantum physics [90]. How do the wave and particle description interact with each other? Where does the quantum world stop and the macro world begin [91]? Why do we need to describe our particles with quantum mechanics and our detectors as classical measuring devices?

Interpretations of quantum physics try to answer these questions by contextualising the mathematical equations and interpret how they connect to our observed reality [92]. On the contrary, we can also apply these equations to predict outcomes of experiments without assuming that they represent an entity in the world. This would imply that quantum physics is just an epistemic tool to describe the world without any ontic conceptions. Different interpretations of quantum physics can be split in two contradicting groups. Of course, there is always heterogeneity in each group and they might be not strictly separable but this will serve as a general overview of how to explain the detection of an interference pattern in our experiments.

1. **epistemic Ψ:** the first group considers the wave function to be epistemic, meaning that it is just a scientific representation of an underlying process and does not describe a real physical state [93]. The wave function can be used to give predictions about measurement results but does not describe a real phenomenon. This conception adopted by the Copenhagen interpretation and Qbism has been famously criticised by Einstein, who considered such a theory to be an incomplete description of the world [94].

2. **ontic Ψ:** the second group assumes that the wave function is not only a description of the world but also hints at deeper processes that explain wave function collapse and the relation between the atomic and the macro world. This view

has been adopted by Bohmian Mechanics [95] and the Many-Worlds interpretation [96].

A different way of making sense of the quantum to classical transition are non-linear extensions to the Schrödinger equation. In contrast to other interpretations, these models give slightly different experimental predictions and can therefore be tested in matter-wave interferometry.

A.2 Copenhagen Interpretation

Accredited to Bohr and Heisenberg, the Copenhagen interpretation provides the textbook way of understanding quantum physics. It assumes wave-particle complementarity and gives a straightforward way of applying this principle to our matter-wave experiments. In this interpretation, the molecules in our apparatus are described by probability waves that extend over multiple slits. The wave just gives a stochastic description of where the particle could be but does not say anything about the actual position. It is assumed that the particle is delocalised over multiple slits. A linear superposition of possible locations collapses in the moment of interaction with a macroscopic device - in our case the molecule detector. This leads to non-deterministic evolution of the system and the irreversibility of measurements [86]. To sum up, in the Copenhagen picture we have to treat our molecules and detectors with two different sets of laws. The molecules are represented by the probability wave Ψ and the detector is described by classical physics. The interaction of the micro and the macro world leads to the detection of determined particle positions. The interpretation does not explain why both scales have to be treated differently.

Modern versions of this interpretation take information to be a crucial quantity to understand the behaviour of matter-waves [97]. Brukner and Zeilinger assume that which-path information - the possibility to detect through which slit the particle went - leads to decoherence and subsequently to the disappearance of the interference pattern.

Additionally, Feynman's path-integral formulation can be understood as an extension of the Copenhagen interpretation [98]. It explains the wave behaviour in a matter-wave experiment as a summation over all possible trajectories. These paths, no matter how surreal they might look, amplify and cancel each other out to yield the observed interference pattern in the end.

A.3 Relational Interpretation

In the 1990s, Rovelli proposed an extension of the copenhagen picture that highlights the role of the observer in quantum physics [99]. His relational interpretation assumes every interaction to be an act of observation connecting the observer and the observed. A measurement does not reveal a predetermined property of the observed but only has meaning in relation to the observation. It is important to add that every interaction is an observation and that everything can act as an observing agent: a photon, a detector, and scientists.

For a matter-wave experiment, the interpretation gives a straight-forward point-of-view. If an observation happens at one of the slits, the interaction of the photon and the molecule includes information about which slit it went through. If the observation happened at the detector after the slits, no such information exists. But this description also includes that the observer (photons) and the observed (molecules) are non-separable. It is therefore meaningless to ask what happens to the particles if we do not measure them. By only looking at relations we have to acknowledge that space and time are not real entities but just exist in relation to our measurements. A molecule can appear to go "through two slits at once" because the spatial relations are identical in our experiment.

A.4 Many Worlds

Another prominent way to interpret the equations of quantum mechanics has been devised by Everett [96]. He termed it the relative state interpretation but recent proponents usually refer to it as Many-Worlds interpretation. In this framework, the wave function Ψ is taken as a real description of a physical system. A linear superposition of the quantum state does not describe possible locations but actual ones. And the measurement of a superposition does not induce wave function collapse but selects a world in which the observed outcome is realised. All other outcomes are also physically real but in different branches of the universe [100].

In this interpretation, collapse of the wave function is explained by continuous branching of worlds. Every quantum measurement creates new branches in which all possibilities are realised. But, experimentally we only have access to a single world. A matter-wave interferometer would therefore be explained by different branches interacting with each other. The interference pattern arises because in every branch the

particle goes through a different slit. After detection, the branches decohere and can not interact any more. By assuming a huge number of world branches, we can circumvent many quantum paradoxes but there is no experimental test of this speculated multiplicity of universes. Nevertheless, Deutsch argues that the double-slit experiment is evidence that different particles from different worlds interact with each other [100].

A.5 De Broglie-Bohm Theory

The second well-known ontic interpretation of quantum physics is called de Broglie-Bohm Theory. First developed by de Broglie and later extended by Bohm, the model assumes the wave function and the particles to be real physical systems [95]. In this interpretation, the locations of particles are always clearly determined and the velocities of particles are guided by the wave function. The dynamics are a physical interaction of particle and wave. Because the complex wave guides the localised particle the interpretation is also known as pilot-wave theory.

In contrast to other explanations, the model is based on the assumption of non-local hidden variables. The position of particles are always given but can not be measured to infinite precision.

Proponents of the interpretation highlight its deterministic and realist properties. It is therefore possible to calculate exact trajectories of the particles in a matter-wave interferometer [101]. But through the non-local interactions of particles and waves these trajectories can only be drawn after the detection. It is therefore an open question if such trajectories play a physical role or are just reconstructions of classical properties that do not have any significance in quantum physics.

A.6 QBism

A novel epistemic interpretation has gained a lot of interest among physicists lately. Fuchs explains quantum physics as a theory in the spirit of Bayesian probability theory [102]. In his view, probabilities arising due to experimental descriptions with the quantum state Ψ do not correspond to anything objective in the world that is independent of observation. The probabilities are descriptions of a degree of belief of an observer [103].

Just like in Bayesian probability theory these subjective laws can be used to predict the outcome of an experiment but only on the given information that the observer

possesses. Making a measurement at a slit or observing the disappearance of the interference pattern is therefore an updating of our knowledge and not a real collapse of the wave function. QBism shows that the equations of quantum physics can be reconstructed by assuming that an observer develops a coherent picture of the experimental results [104]. If she updates her beliefs according to Bayes theorem and creates a coherent set of predictions - also known as the Dutch Book argument - the quantum laws are a sufficient description of her knowledge. In this view, quantum physics is still a complete theory describing all the novel effects we observe in experiments but it is more a description of how we make sense of the world than how the world behaves independently of us [105].

A.7 Collapse Models

The last sections described different interpretations of the same mathematical equations that make up quantum physics. Even though they all give completely different accounts of how to understand our observations, they are so far indistinguishable in experiment. In contrast, collapse models propose modifications of the Schrödinger equation to explain the quantum to classical transition. Continuous Spontaneous Localisation (CSL) is today the best candidate for a collapse model [10]. It explains the quantum to classical transition by proposing a continuous process that localises particles and destroys the superposition after a given time automatically. The bigger the quantum system and the further the superposition spreads the faster this process takes place.

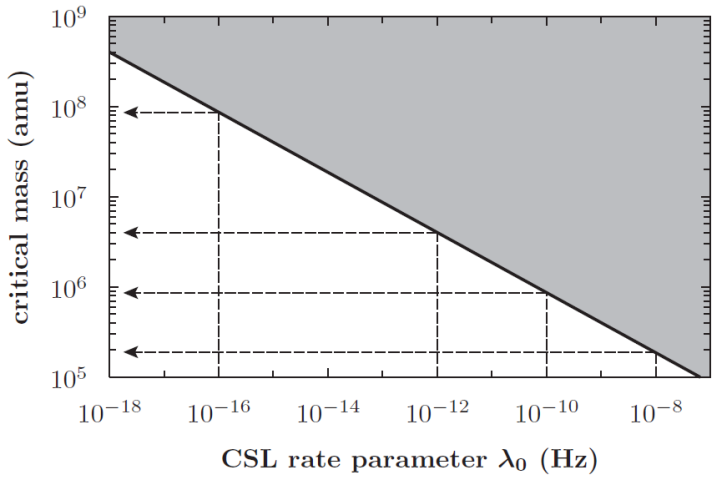

Figure 31: **Classes of localisation theories that can be ruled out by molecule interferometry.** *The grey area is the proposed regime by which interference of high-mass particles should be forbidden. The localisation parameter λ_0 gives the rate at which the quantum to classical transition takes place.* Adapted from [106]

The localisation is modelled by a non-linear extension to the Schrödinger equation, which represents a stochastic field continuously interacting with the quantum state. Because of this modification of the usual quantum laws, the theory predicts the complete disappearance of interference fringes for bigger quantum systems. Therefore, we can use matter-wave interferometry to test different modifications. If we are able to observe high-mass interference we continuously rule out more and more possible parameters for CSL.

A.8 Fundamental Questions and Experiment

Even though matter-wave experiments have been performed for nearly a century, there are still many open questions of how to interpret the interference pattern and what the wave function Ψ represents. Is it the description of real physical systems or an epistemic tool to predict experimental results? Nevertheless, I tried to give an overview over different explanations and showed how high-mass interferometry could gather new insights into these fundamental questions. Most interpretations assume that quantum physics is universally valid and complete. The only difference lies in the way they describe the appearance of the classical measurement results out of the

quantum equations.

The usual stance of researchers is that experimental progress in quantum physics can be made without committing to a specific interpretation, but we as scientists have to be aware about the ambiguities of our language and the open questions concerning the foundations of interferometry. It is therefore important to be critical about one's assumptions and to keep asking fundamental questions even when developing new practical applications for matter-wave experiments.

References

1. Planck, M. Zur Theorie des Gesetzes der Energieverteilung im Normalspectrum. *Verhandlungen der Deutschen Physikalischen Gesellschaft* **17,** 237–245 (1900).
2. Broglie, L. D. Waves and Quanta. *Nature* **112** (1923).
3. Davisson, C. & Germer, L. H. Diffraction of Electrons by a Crystal of Nickel. *Physical Review* **30,** 705–740 (1927).
4. Arndt, M. *et al.* Wave–Particle Duality of C60 Molecules. *Nature* **401,** 680–682 (1999).
5. Fein, Y. Y. *et al.* Quantum Superposition of Molecules Beyond 25 kDa. *Nature Physics* **15,** 1242–1245 (2019).
6. Mairhofer, L. *et al.* Quantum-Assisted Metrology of Neutral Vitamins in the Gas Phase. *Angewandte Chemie International Edition* **56,** 10947–10951 (2017).
7. Kialka, F. *et al.* Concepts for Long-Baseline High-Mass Matter-Wave Interferometry. *Physica Scripta* **94,** 034001 (2019).
8. Bynum, W. A History of Molecular Biology. *Nature Medicine* **5,** 140–140. (2020) (1999).
9. McFadden, J. & Al-Khalili J. The origins of quantum biology. *Proceedings of the Royal Society A: Mathematical, Physical and Engineering Sciences* **474,** 20180674. (2019) (2018).
10. Bassi, A., Lochan, K., Satin, S., Singh, T. P. & Ulbricht, H. Models of Wavefunction Collapse, Underlying Theories, and Experimental Tests. *Reviews of Modern Physics* **85,** 471–527 (2013).
11. Kallmann, H. & Reiche, F. Über den Durchgang bewegter Moleküle durch inhomogene Kraftfelder. *Zeitschrift für Physik* **6,** 352–375. ISSN: 0044-3328. (2020) (1921).
12. Wrede, E. Über die Ablenkung von Molekularstrahlen elektrischer Dipolmoleküle im inhomogenen elektrischen Feld. *Zeitschrift für Physik* **44,** 261–268. (2020) (1927).
13. Gerlach, W. & Stern, O. Das magnetische Moment des Silberatoms. *Zeitschrift für Physik* **9,** 353–355 (1922).

14. Friedrich, B. & Herschbach, D. Stern and Gerlach: How a Bad Cigar Helped Reorient Atomic Physics. *Physics Today* **56,** 53 (2007).

15. Schmid, P., Stöhr, F., Arndt, M., Tüxen, J. & Mayor, M. Single-Photon Ionization of Organic Molecules Beyond 10 kDa. *Journal of the American Society for Mass Spectrometry* **24.** Publisher: American Chemical Society, 602–608 (2013).

16. Van de Meerakker, S. Y. T., Bethlem, H. L., Vanhaecke, N. & Meijer, G. Manipulation and Control of Molecular Beams. *Chemical Reviews* **112,** 4828–4878 (2012).

17. Posthumus, M. A., Kistemaker, P. G., Meuzelaar, H. L. C. & Ten Noever de Brauw, M. C. Laser desorption-mass spectrometry of polar nonvolatile bioorganic molecules. *Analytical Chemistry* **50.** Publisher: American Chemical Society, 985–991 (1978).

18. Weinkauf, R., Aicher, P., Wesley, G., Grotemeyer, J. & Schlag, E. W. Femtosecond versus Nanosecond Multiphoton Ionization and Dissociation of Large Molecules. *The Journal of Physical Chemistry* **98,** 8381–8391 (1994).

19. Schlag, E. W., Grotemeyer, J. & Levine, R. D. Do large molecules ionize? *Chemical Physics Letters* **190,** 521–527. (2020) (1992).

20. Wysocki, V. H., Resing, K. A., Zhang, Q. & Cheng, G. Mass spectrometry of peptides and proteins. *Methods* **35,** 211–222 (2005).

21. Grotemeyer, J. & Schlag, E. W. *Biomolecules in the gas phase: multiphoton ionization mass spectrometry* Publisher: American Chemical Society.

22. Sezer, U. *et al.* Selective Photodissociation of Tailored Molecular Tags as a Tool for Quantum Optics. *Beilstein Journal of Nanotechnology* **8,** 325–333 (2017).

23. Brodbelt, J. S. Photodissociation Mass Spectrometry: New Tools for Characterization of Biological Molecules. *Chem. Soc. Rev.* **43,** 2757–2783 (2014).

24. Sleno, L. & Volmer, D. A. Ion activation methods for tandem mass spectrometry. *Journal of Mass Spectrometry* **39,** 1091–1112 (2004).

25. Debiossac, M. *et al.* Tailored Photocleavable Peptides: Fragmentation and Neutralization Pathways in High Vacuum. *Physical Chemistry Chemical Physics* **20,** 11412–11417 (2018).

26. Woodin, R. L., Bomse, D. S. & Beauchamp, J. L. in *Chemical and Biochemical Applications of Lasers* (ed Moore, C. B.) 355–388 (Academic Press, 1979). (2020).

27. Robertson, E. G. & Simons, J. P. Getting into shape: Conformational and supramolecular landscapes in small biomolecules and their hydrated clusters. *Physical Chemistry Chemical Physics* **3,** 1–18 (2001).

28. Ly, T. & Julian, R. R. Residue-Specific Radical-Directed Dissociation of Whole Proteins in the Gas Phase. *Journal of the American Chemical Society* **130,** 351–358 (2008).

29. Nimmrichter, S., Hornberger, K., Ulbricht, H. & Arndt, M. Absolute absorption spectroscopy based on molecule interferometry. *Physical Review A* **78,** 063607 (2008).

30. Gring, M. *et al.* Influence of conformational molecular dynamics on matter wave interferometry. *Physical Review A* **81,** 031604 (2010).

31. Young, T. *A Course of Lectures on Natural Philosophy and the Mechanical Arts* (University of California Libraries, London, 1807).

32. Brand, C., Sezer, U., Arndt, M. & Eibenberger, S. in *Current Trends in Atomic Physics* (ed Browaeys, A.) (Oxford University Press, 2019).

33. Clauser, J. F. & Li, S. Talbot-von Lau Atom Interferometry with Cold Slow Potassium. *Physical Review A* **49,** 2213–2216 (1994).

34. Case, W. B., Tomandl, M., Deachapunya, S. & Arndt, M. Realization of Optical Carpets in the Talbot and Talbot-Lau Configurations. *Optics Express* **17,** 1–9 (2009).

35. Kapitza, P. L. & Dirac, P. a. M. The Reflection of Electrons from Standing Light Waves. *Mathematical Proceedings of the Cambridge Philosophical Society* **29,** 297–300 (1933).

36. Nairz, O., Brezger, B., Arndt, M. & Zeilinger, A. Diffraction of Complex Molecules by Structures Made of Light. *Physical Review Letters* **87,** 160401 (2001).

37. Dörre, N. *et al.* Photofragmentation Beam Splitters for Matter-Wave Interferometry. *Physical Review Letters* **113,** 1–5 (2014).

38. Hell, S. W. & Wichmann, J. Breaking the Diffraction Resolution Limit by Stimulated Emission: Stimulated-Emission-Depletion Fluorescence Microscopy. *Optics Letters* **19,** 780–782. (2019) (1994).

39. Taylor, R. W. & Sandoghdar, V. Interferometric Scattering (iSCAT) Microscopy & Related Techniques. *arXiv:1812.10765 [cond-mat, physics:physics]* (Dec. 27, 2018).

40. Gemeinhardt, A. *et al.* Label-Free Imaging of Single Proteins Secreted from Living Cells via iSCAT Microscopy. *Journal of Visualized Experiments,* 58486 (2018).

41. Wolff, M. M. & Stephens, W. E. A Pulsed Mass Spectrometer with Time Dispersion. *Review of Scientific Instruments* **24,** 616–617 (1953).

42. Douglas, D. J. & French, J. B. Collisional focusing effects in radio frequency quadrupoles. *Journal of the American Society for Mass Spectrometry* **3,** 398–408 (1992).

43. Egorov, D., Lahaye, T., Schöllkopf, W., Friedrich, B. & Doyle, J. M. Buffer-gas cooling of atomic and molecular beams. *Physical Review A* **66.** Publisher: American Physical Society, 043401 (2002).

44. Hackermueller, L. *et al.* The Wave Nature of Biomolecules and Fluorofullerenes. *Physical Review Letters* **91,** 1–5 (2003).

45. Eibenberger, S., Gerlich, S., Arndt, M., Mayor, M. & Tüxen, J. Matter–Wave Interference of Particles Selected From a Molecular Library with Masses Exceeding 10000 amu. *Physical Chemistry Chemical Physics* **15,** 14696–14700 (2013).

46. *PDB101: Global Health: Diabetes Mellitus: Drugs: Insulin* accessed: 2020-08-27. http://pdb101.rcsb.org/global-health/diabetes-mellitus/drugs/insulin/insulin.

47. Fenn, J. B., Mann, M., Meng, C. K., Wong, S. F. & Whitehouse, C. M. Electrospray Ionization for Mass Spectrometry of Large Biomolecules. *Science* **246,** 64–71 (1989).

48. Hainfeld, J. F., Wall, J. S. & Wang, K. Titin: Quantitative Mass Measurements by Scanning Transmission Electron Microscopy and Structural Implications for the Sarcomere Matrix of Skeletal Muscle. *FEBS Letters* **234,** 145–148 (1988).

49. Pace, C. N., Vajdos, F., Fee, L., Grimsley, G. & Gray, T. How to Measure and Predict the Molar Absorption Coefficient of a Protein. *Protein Science* **4,** 2411–2423 (1995).

50. Dole, M. *et al.* Molecular Beams of Macroions. *The Journal of Chemical Physics* **49,** 2240–2249 (1968).

51. Fenn, J. B. Electrospray Wings for Molecular Elephants. *Angewandte Chemie International Edition* **42,** 3871–94 (2002).

52. Taylor Geoffrey Ingram. Disintegration of Water Drops in an Electric Field. *Proceedings of the Royal Society of London. Series A. Mathematical and Physical Sciences* **280,** 383–397 (1964).

53. Banerjee, S. & Mazumdar, S. Electrospray Ionization Mass Spectrometry: A Technique to Access the Information beyond the Molecular Weight of the Analyte. *International Journal of Analytical Chemistry,* 1–41 (2012).

54. Jaworek, A. & Krupa, A. Jet and Drops Formation in Electrohydrodynamic Spraying of Liquids. A Systematic Approach. *Experiments in Fluids* **27,** 43–52 (1999).

55. Wilm, M. Principles of Electrospray Ionization. *Molecular & Cellular Proteomics* **10,** 1–8 (2011).

56. Konermann, L., Ahadi, E., Rodriguez, A. D. & Vahidi, S. Unraveling the Mechanism of Electrospray Ionization. *Analytical Chemistry* **85,** 2–9 (2013).

57. Iribarne, J. V. & Thomson, B. A. On the Evaporation of Small Ions from Charged Droplets. *The Journal of Chemical Physics* **64,** 2287–2294 (1976).

58. Nguyen, S. & Fenn, J. B. Gas-phase Ions of Solute Species from Charged Droplets of Solutions. *Proceedings of the National Academy of Sciences of the United States of America* **104,** 1111–1117 (2007).

59. Wilm, M. & Mann, M. Analytical Properties of the Nanoelectrospray Ion Source. *Analytical Chemistry* **68,** 1–8 (1996).

60. Karas, M., Bachmann, D. & Hillenkamp, F. Influence of the Wavelength in High-Irradiance Ultraviolet Laser Desorption Mass Spectrometry of Organic Molecules. *Analytical Chemistry* **57,** 2935–2939 (1985).

61. Knochenmuss, R. The Coupled Chemical and Physical Dynamics Model of MALDI. *Annual Review of Analytical Chemistry* **9,** 365–385 (2016).

62. Tanaka, K. *et al.* Protein and Polymer Analyses up to m/z 100 000 by Laser Ionization Time-of-Flight Mass Spectrometry. *Rapid Communications in Mass Spectrometry* **2,** 151–153 (1988).

63. Tol, B. D. M. v., Geurink, P. P. & Ovaa, H. A MALDI-TOF Approach to Ubiquitin Ligase Activity. *Cell Chemical Biology* **25,** 1053–1055 (2018).

64. Bouakil, M. *et al.* Visible Multiphoton Dissociation of Chromophore-Tagged Peptides. *Journal of The American Society for Mass Spectrometry* **28,** 2181–2188 (2017).

65. Wells, J. M. & McLuckey, S. A. Collision-Induced Dissociation (CID) of Peptides and Proteins. *Methods in Enzymology* **402,** 148–185 (2005).

66. Lermyte, F., Williams, J. P., Brown, J. M., Martin, E. M. & Sobott, F. Extensive Charge Reduction and Dissociation of Intact Protein Complexes Following Electron Transfer on a Quadrupole-Ion Mobility-Time-of-Flight MS. *Journal of The American Society for Mass Spectrometry* **26,** 1068–1076 (2015).

67. Hayter, J. R., Robertson, D. H. L., Gaskell, S. J. & Beynon, R. J. Proteome Analysis of Intact Proteins in Complex Mixtures. *Molecular & Cellular Proteomics* **2,** 85–95 (2003).

68. Frey, B. L., Lin, Y., Westphall, M. S. & Smith, L. M. Controlling Gas-Phase Reactions for Efficient Charge Reduction Electrospray Mass Spectrometry of Intact Proteins. *Journal of the American Society for Mass Spectrometry* **16,** 1876–1887 (2005).

69. Kerschbaum, M. *Charge Reduction of Electrospray Ionized Biomolecules Using Corona Discharge.* Bachelor Thesis. (University of Vienna, Department of Physics, 2018).

70. Chen, J. & Davidson, J. H. Electron Density and Energy Distributions in the Positive DC Corona: Interpretation for Corona-Enhanced Chemical Reactions. *Plasma Chemistry and Plasma Processing* **22,** 199–224 (2002).

71. Fernandez de la Mora, J. Mobility Analysis of Proteins by Charge Reduction in a Bipolar Electrospray Source. *Analytical Chemistry* **90,** 12187–12190 (2018).

72. Brunet, C. *et al.* Photo-Induced Electron Detachment of Protein Polyanions in the VUV Range. *The Journal of Chemical Physics* **138,** 064301 (2013).

73. Antoine, R. & Dugourd, P. Visible and Ultraviolet Spectroscopy of Gas Phase Protein Ions. *Physical Chemistry Chemical Physics* **13,** 16494–16509. (2019) (2011).

74. Mamyrin, B. Time-of-Flight Mass Spectrometry (concepts, achievements, and prospects). *International Journal of Mass Spectrometry* **206,** 251–266 (2001).

75. Mamyrin, B. A., Karataev, V. I., Shmikk, D. V. & Zagulin, V. A. The Mass-Reflectron, a New Nonmagnetic Time-of-Flight Mass Spectrometer with High Resolution. *Soviet Physics - JETP* **37,** 45–48 (1973).

76. *Waters Q-Tof User's Guide* 2nd ed. (Micromass UK Limited, Wythenshawe, 2003).

77. Kolb, H. C., Finn, M. G. & Sharpless, K. B. Click Chemistry: Diverse Chemical Function from a Few Good Reactions. *Angewandte Chemie International Edition* **40,** 2004–2021 (2001).

78. Debiossac, M. *et al.* Supplementary Information: Tailored Photocleavable Peptides: Fragmentation and Neutralization Pathways in High Vacuum. *Physical Chemistry Chemical Physics* **20,** 11412–11417 (2018).

79. Schätti, J. *Towards Matter-Wave Experiments with Biomolecules: Generation and Detection of Neutral Biomolecular Beams.* PhD thesis (University of Basel, Department of Chemistry, 2019).

80. Schätti, J. *et al.* Neutralization of insulin by photocleavage under high vacuum. *Chemical Communications* **55,** 12507–12510 (2019).

81. Fan, X. Z. *et al.* Tobacco Mosaic Virus: A Biological Building Block for Micro/Nano/Bio Systems. *Journal of Vacuum Science & Technology A* **31,** 050815 (2013).

82. Kriegleder, M. *Soft Desorption of Viruses for Quantum Interferometry.* Bachelor Thesis (University of Vienna, Department of Physics, 2017).

83. Hanley, L. & Zimmermann, R. Light and Molecular Ions: The Emergence of Vacuum UV Single-Photon Ionization in MS. *Analytical Chemistry* **81,** 4174–4182 (2009).

84. Brismar, H, Trepte, O & Ulfhake, B. Spectra and Fluorescence Lifetimes of Lissamine Rhodamine, Tetramethylrhodamine Isothiocyanate, Texas Red, and Cyanine 3.18 Fluorophores: Influences of Some Environmental Factors Recorded with a Confocal Laser Scanning Microscope. *Journal of Histochemistry & Cytochemistry* **43,** 699–707 (1995).

85. Rodewald, J. *et al.* in *Exploring the World with the Laser: Dedicated to Theodor Hänsch on his 75th birthday* (eds Meschede, D., Udem, T. & Esslinger, T.) 21–34 (2018).

86. Bohr, N. *Atomic Theory and the Description of Nature* (Ox Bow Press, 1934).

87. Howard, D. Who Invented the “Copenhagen Interpretation”? A Study in Mythology. *Philosophy of Science* **71,** 669–682 (2004).

88. Wootters, W. K. & Zurek, W. H. Complementarity in the Double-Slit Experiment: Quantum Nonseparability and a Quantitative Statement of Bohr’s Principle. *Physical Review D* **19,** 473–484 (1979).

89. Feynman, R., Leighton, R & Sands, M. *The Feynman Lectures on Physics* (Addison-Wesley, Reading, 1965).

90. Zeh, H. On the Interpretation of Measurement in Quantum Theory. *Foundations of Physics* **1,** 69–76 (1970).

91. Zurek, W. H. Decoherence, Einselection, and the Quantum Origins of the Classical. *Reviews of Modern Physics* **75,** 715–775 (2003).

92. Myrvold, W. & Zalta, E. N. *Philosophical Issues in Quantum Theory.* The Stanford Encyclopedia of Philosophy. `https://plato.stanford.edu/archives/fall2018/entries/qt-issues/accessed:6.6.2019` (2019).

93. Spekkens, R. W. In Defense of the Epistemic View of Quantum States: a Toy Theory. *Physical Review A* **75,** 032110 (2007).

94. Einstein, A., Podolsky, B. & Rosen, N. Can Quantum-Mechanical Description of Physical Reality Be Considered Complete? *Physical Review* **47,** 777–780 (1935).

95. Bohm, D. A Suggested Interpretation of the Quantum Theory in Terms of "Hidden" Variables. I. *Physical Review* **85,** 166–179 (1952).

96. Everett, H. "Relative State" Formulation of Quantum Mechanics. *Reviews of Modern Physics* **29,** 454–462 (1957).

97. Brukner, & Zeilinger, A. in *Time, Quantum and Information* (eds Castell, L. & Ischebeck, O.) 323–354 (Springer, Berlin, Heidelberg, 2003).

98. Feynman, R. P. Space-Time Approach to Non-Relativistic Quantum Mechanics. *Reviews of Modern Physics* **20,** 367–387 (1948).

99. Rovelli, C. Relational Quantum Mechanics. *International Journal of Theoretical Physics* **35,** 1637–1678 (1996).

100. Deutsch, D. *The Fabric of Reality* (Viking Adult, London, 1997).

101. Philippidis, C., Dewdney, C. & Hiley, B. J. Quantum Interference and the Quantum Potential. *Il Nuovo Cimento B Series 11* **52,** 15–28 (1979).

102. Fuchs, C. A. & Schack, R. Quantum-Bayesian Coherence: The No-Nonsense Version. *Reviews of Modern Physics* **85,** 1693–1715 (2013).

103. Fuchs, C. A. & Stacey, B. C. QBism: Quantum Theory as a Hero's Handbook. *arXiv:1612.07308 [quant-ph]* (2019).

104. Fuchs, C. A., Mermin, N. D. & Schack, R. An Introduction to QBism with an Application to the Locality of Quantum Mechanics. *American Journal of Physics* **82,** 749–754 (2014).

105. Fuchs, C. A. On Participatory Realism. *arXiv:1601.04360 [quant-ph]* (2016).

106. Nimmrichter, S., Hornberger, K., Haslinger, P. & Arndt, M. Testing Spontaneous Localization Theories with Matter-Wave Interferometry. *Physical Review A* **83,** 043621 (2011).